JOURNAL OF GEOPHYSICAL RESEARCH, VOL. 114, C04019, doi:10.1029/2008JC004995, 2009

Radiative and turbulent surface heat fluxes over sea ice in the western Weddell Sea in early summer

Timo Vihma,[1] Milla M. Johansson,[2,3] and Jouko Launiainen[2,4]

Received 30 June 2008; revised 2 January 2009; accepted 25 February 2009; published 25 April 2009.

[1] The radiative and turbulent heat fluxes between the snow-covered sea ice and the atmosphere were analyzed on the basis of observations during the Ice Station Polarstern (ISPOL) in the western Weddell Sea from 28 November 2004 to 2 January 2005. The net heat flux to the snowpack was 3 ± 2 W m^{-2} (mean ± standard deviation; defined positive toward snow), consisting of the net shortwave radiation (52 ± 8 W m^{-2}), net longwave radiation (-29 ± 4 W m^{-2}), latent heat flux (-14 ± 5 W m^{-2}), and sensible heat flux (-6 ± 5 W m^{-2}). The snowpack receives heat at daytime while releases heat every night. Snow thinning was due to approximately equal contributions of the increase of snow density, melt, and evaporation. The surface albedo only decreased from 0.9 to 0.8. During a case of cold air advection, the sensible heat flux was even below -50 W m^{-2}. At night, the snow surface temperature was strongly controlled by the incoming longwave radiation. The diurnal cycle in the downward solar radiation drove diurnal cycles in 14 other variables. Comparisons against observations from the Arctic sea ice in summer indicated that at ISPOL the air was colder, surface albedo was higher, and a larger portion of the absorbed solar radiation was returned to the atmosphere via turbulent heat fluxes. The limited melt allowed larger diurnal cycles. Due to regional differences in atmospheric circulation and ice conditions, the ISPOL results cannot be fully generalized for the entire Antarctic sea ice zone.

Citation: Vihma, T., M. M. Johansson, and J. Launiainen (2009), Radiative and turbulent surface heat fluxes over sea ice in the western Weddell Sea in early summer, *J. Geophys. Res.*, *114*, C04019, doi:10.1029/2008JC004995.

1. Introduction

[2] The Antarctic sea ice cover has a strong influence on the dynamics and thermodynamics of the atmosphere [*Valkonen et al.*, 2008] and ocean [*Martinson and Iannuzzi*, 1998; *Stössel et al.*, 2008], as well as on various biogeochemical processes in the ocean [*Thomas and Dieckmann*, 2003]. In winter the sea ice cover acts as an effective insulator between the cold atmosphere and the relatively warm ocean. In summer, the thermal differences are much smaller, but the radiative and turbulent fluxes to snow and ice surface control the melt: 80% of the Antarctic sea ice melts each summer, the extent of the sea ice zone decreasing from 19×10^6 km^2 in winter to 3.5×10^6 km^2 in summer [*Parkinson*, 2004]. Quantitative knowledge on the radiative and turbulent surface fluxes over Antarctic sea ice is, however, still very limited.

[3] The sea-ice cover consists of ice floes of varying thickness, typically covered by snow, and is broken by cracks, leads and polynyas: the ice conditions are controlled by a close interaction of dynamic and thermodynamic processes [*Haas*, 2003]. The thermal stratification of the atmospheric boundary layer (ABL) over sea ice varies in space and time, being affected by the ice thickness and presence of open water as well as by the diurnal cycle of solar radiation and seasonal and synoptic-scale changes in the weather conditions. According to year-round observations over the Arctic sea ice, the stratification is typically stable during winter and near-neutral during summer [*Persson et al.*, 2002; *Grachev et al.*, 2005]. In the Antarctic, the sea ice zone surrounds the continent: the sea ice cover is on average thinner, the ice concentration is lower, the sea ice zone locates at lower latitudes than in the Arctic, and the katabatic winds advect cold continental air masses over the sea ice. These factors tend to reduce the thermal stratification, and its temporal and spatial distribution is not well known.

[4] The cloud cover has a dominating influence on the shortwave and longwave radiative fluxes at the snow/ice surface. Due to its opposite effects on shortwave and longwave radiation, the cloud forcing on the surface temperature can be either positive or negative depending on the season and latitude. The net solar radiation at the snow/ice surface is also strongly controlled by the surface albedo, ranging from 0.9 for dry new snow to 0.4 for melting bare ice [*Perovich*, 1996], which results in a strong feedback on the snow and ice melt.

[5] Observations of turbulent and radiative surface fluxes over Antarctic sea ice have been rare. Direct flux measurements over sea ice have been made in February–May 1992

[1] Meteorological Research, Finnish Meteorological Institute, Helsinki, Finland.
[2] Finnish Institute of Marine Research, Helsinki, Finland.
[3] Now at Marine Research, Finnish Meteorological Institute, Helsinki, Finland.
[4] Retired.

0148-0227/09/2008JC004995$09.00

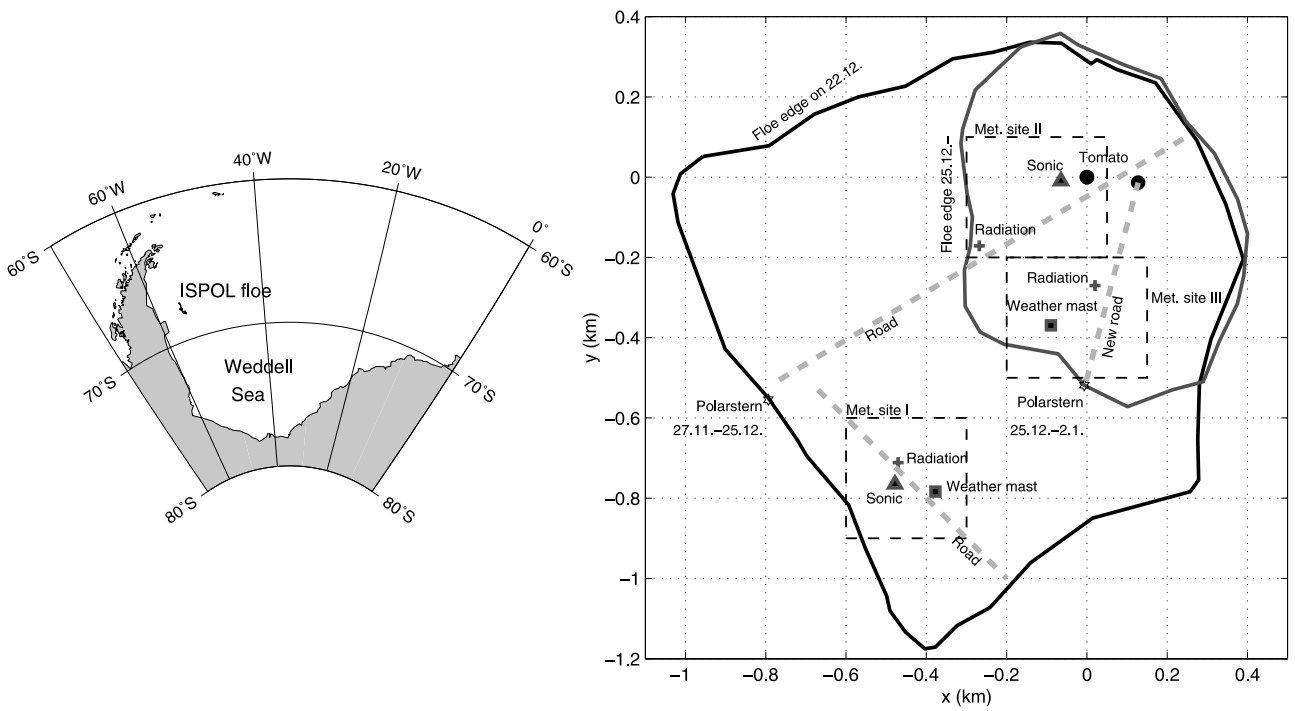

Figure 1. (left) Drift trajectory of the ISPOL floe in the Weddell Sea and (right) map of the ISPOL floe with the measurement sites (coordinates provided by Miles McPhee).

on the Ice Station Weddell (ISW [*Andreas et al.*, 2000, 2004, 2005]). In addition, radiative fluxes have been measured onboard ships cruising in the sea ice zone [*Wendler et al.*, 1997, 2005; *Wendler and Worby*, 2001; *Brandt et al.*, 2005]. Indirect estimates on turbulent fluxes have been made on the basis of ship observations mostly in summer [*Andreas*, 1985; *Wendler et al.*, 2005], wind and temperature measurements from drifting buoys [*Kottmeier and Engelbart*, 1992; *Launiainen and Vihma*, 1994; *Vihma et al.*, 2002], and kite measurements applying a budget method for fluxes over leads [*Guest*, 2007].

[6] In this paper, we analyze observations on the radiative and turbulent surface fluxes over the Weddell Sea ice cover in austral spring and early summer, from 28 November 2004 to 2 January 2005. The observations were made at the drifting Ice Station Polarstern (ISPOL [*Hellmer et al.*, 2008]), which was an interdisciplinary project primarily organized by the Alfred Wegener Institute for Polar and Marine Research (AWI), Germany, with participants from 11 countries. The focus of the field experiment was on physical and biological processes in sea ice and the air-ice-ocean interaction. Considering the physical processes, the ISPOL expedition has yielded results on meteorology [*Bareiss and Görgen*, 2008], sea ice dynamics [*Steer et al.*, 2008; *Heil et al.*, 2008], properties and thermodynamics of snow and sea ice [*Willmes et al.*, 2006; *Nicolaus et al.*, 2006; *Haas et al.*, 2008; *Tison et al.*, 2008; M. Nicolaus et al., Evolution of first- and second-year snow properties on sea ice in the Weddell Sea during spring-summer transition, submitted to *Journal of Geophysical Research*, 2009, hereinafter referred to as Nicolaus et al., submitted manuscript, 2009], and air-ocean exchange [*McPhee*, 2008].

[7] The objectives of this paper are (1) to quantify the shortwave and longwave radiative fluxes and the turbulent fluxes of sensible and latent heat over Antarctic sea ice in early summer, (2) to analyze the interaction between the cloud cover, near-surface wind, air temperature and humidity, and the surface fluxes, and (3) to evaluate the differences in these processes between the Arctic and Antarctic sea ice zones. Attention is paid on the diurnal cycles of the atmospheric and surface variables as well as on the processes resulting in extreme values of temperatures and fluxes. The observations and calculation methods are presented in section 2, time series of the fluxes in section 3, and the diurnal cycles in section 4. The results are evaluated and compared against previous studies in section 5, and conclusions are drawn in section 6.

2. Observations and Methods

2.1. Observation Sites and Weather Conditions

[8] The ISPOL field experiment was mainly conducted on a single ice floe, located around 68°S, 55°W, drifting 290 km during the experiment with a net south-north displacement of 98 km [*Hellmer et al.*, 2006, 2008]. *R/V Polarstern* was moored to the floe. The floe experienced two major breakups during the experiment (on 2 and 24–25 December 2004), being 1.5 × 1.5 km in diameter in early December and finally reducing to 0.7–0.8 km in diameter (Figure 1). The ISPOL floe mostly consisted of 2 m thick second-year sea ice covered by 0.2–1.1 m of snow, interspersed by 0.9–1.8 m thick first-year ice with 0.3 m snow cover [*Hellmer et al.*, 2006]. The snow and ice thicknesses at our measurement sites are presented in Table 1.

[9] An overview of the radiation and turbulent flux measurements carried out by our team (JL and MJ) is presented in Table 1. In addition, snow thickness and density were measured by the AWI group (Nicolaus et al., submitted manuscript, 2009) and us. At Site I we measured the average

Table 1. An Overview of the Measurement Sites and Equipment Used

Site, Floe, and Ice/Snow Properties	Equipment	Measurement Quantities	Period	Sampling/Registration Rate
I				
Main experiment floe (ø 1.5 km reducing to 0.7–0.8 km), ridges up to 2 m, ice thickness 0.8–1.6 m, snow thickness 0.2–1.1 m	radiation station (Eppley)	shortwave and longwave radiation	28.11–25.12.04	1 min
	radiation station (Kipp&Zonen)	shortwave and longwave radiation	1–4.12.04	1 min
	meteorological mast (Aanderaa sensors)	wind and air temperature profile, relative humidity	29.11–25. 12.04	10 min
	sonic anemometer (Metek USA-1)	momentum and sensible heat flux, turbulence	30.11–25.12.04	20 Hz sampling, 10 min averaging
II				
Main experiment floe, see above, ice thickness 0.8–1.1 m, snow thickness 0.1–0.25 m	radiation station (Kipp & Zonen)	shortwave and longwave radiation	17–26.12.04	1 min
	sonic anemometer (Metek USA-1)	momentum and sensible heat flux, turbulence	18.12.04–2.1.05	20 Hz sampling, 10 min averaging
III				
Main experiment floe, see above, ice thickness 0.8–1.1 m, snow thickness 0.1–0.2 m	radiation station (Kipp&Zonen)	shortwave and longwave radiation	27.12.04–2.1.05	1 min
	meteorological mast (Aanderaa sensors)	wind and air temperature profile, relative humidity	28.12.04–1.1.05	10 min
F				
Vast (3 × 5 km) floe, highly ridged with ridges up to 3 m, ice thickness 1.5–3 m, snow thickness around 0.5 m	radiation station (Kipp&Zonen)	shortwave and longwave radiation	7–15.12.04	1 min
	sonic anemometer (Metek USA-1)	momentum and sensible heat flux, turbulence	6–17.12.04	20 Hz sampling, 10 min averaging

density of the topmost 40–60 cm of snow (usually corresponding to the total snow thickness at the site) by weighing vertical cylindrical samples. At Sites II and III, the density of the total snow column (0.05–0.15 m thick) was measured, but the data turned out to be not accurate enough, as the measurement device was not optimal to sample a thin snowpack. Radiative fluxes, air temperature, relative humidity as well as wind speed and direction were also measured by colleagues from AWI and the University of Trier [*Willmes et al.*, 2006], and the data were compared for quality checking. The results presented in this paper are based on our measurements and *R/V Polarstern* weather station data. Our equipment was spread up on four measurement sites (Table 1, Figure 1), three of which were located on the main experiment floe. One site (F) was set up on a separate floe 10–17 km away from the main floe. Due to technical difficulties and lack of wind and air temperature profile data from Site F, we mostly utilize data from Sites I–III on the main experiment floe.

[10] The weather conditions during the experiment were gentle [*Launiainen et al.*, 2007; *Bareiss and Görgen*, 2008]. The surface wind speed was rather low (2–6 m/s) for most of the period, with only a few days of stronger wind speed related to passing cyclonic depressions (Figure 2a). Northerly and easterly winds were most common (Figure 2b), with some strong warm winds from north or northwest. Cold winds came from over compact sea ice fields in the east or from the continent in the south and southwest. The air temperature was mostly above −5°C (Figure 2c), except of a few cases of cold air advection or a surface-based inversion generated by radiative cooling during clear, calm nights. The first week in December 2004 was the warmest week in the period, with daytime temperatures around 0°C, and a diurnal amplitude of 1°C or less. From 7 to 24 December, high pressure prevailed over the ISPOL region, but was interrupted by a passing low around 20 December. A warm front crossed the region on 25 to 26 December, and a depression stayed over the western Weddell Sea in the end of December.

2.2. Radiation Observations

[11] The incoming and reflected shortwave radiation (Sw_{in} and Sw_{out}, respectively) as well as the incoming and outgoing longwave radiation (Lw_{in} and Lw_{out}) were measured using two sets of equipment. One set consisted of a pair of Kipp & Zonen CM5 pyranometers and a pair of Kipp & Zonen CG2 pyrgeometers, while the other set was equipped with Eppley PSP pyranometers and Eppley PIR pyrgeometers. The sensors were set up at 1.2 m above the snow surface. The data were registered once a minute. The surface albedo was calculated as the ratio of the reflected and incoming shortwave radiation. All fluxes are defined positive downward to the snowpack. On the basis of comparisons against the AWI team observations, the accuracy of the shortwave radiation measurements was approximately 3%. It agrees with previous experiences on the accuracy of similar pyranometers in Antarctic conditions [*Schmidt and König-Langlo*, 1994]. The longwave radiation measurements suffered from the so-called dome heating effect: the shortwave radiation warms up the sensor dome, which emits additional radiation resulting in erroneously large longwave radiation values. The error can be as large as 30 W m^{-2} [e.g., *Fairall et al.*, 1998]. To correct for the dome heating effect, the pyrgeometers were compared against those in the Finnish Meteorological Institute regular radiation measurement station in Jokioinen (WMO station 02963). As a result, correction equations based on the direct and global (diffuse + direct) shortwave radiation were obtained. The corrections for the ISPOL upward and downward longwave radiation were between 0 and 17 W m^{-2}, depending on the shortwave radiation. See sections 2.5 and 3.3 for further analyses on the accuracy of the radiation data.

2.3. Turbulent Flux and Profile Measurements

[12] The sensible heat flux was measured at three sites using two Metek USA-1 sonic anemometers (Table 1). The anemometers were set up on 3.5-m-high steel masts. The instantaneous wind components were logged at 20 Hz frequency, and an averaging time of 10 minutes was used

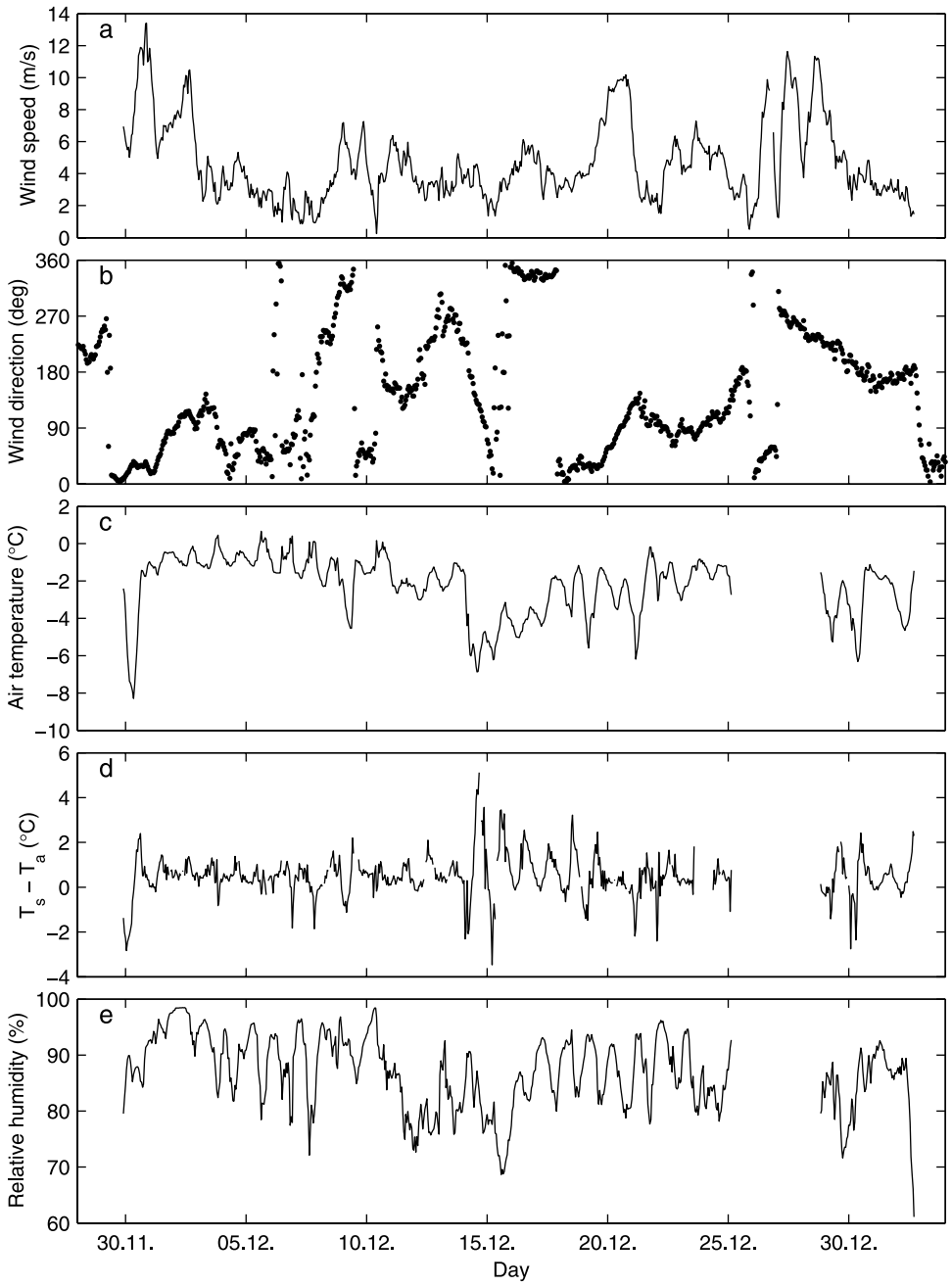

Figure 2. Weather conditions during the ISPOL experiment: (a) wind speed referred to 10 m height based on the meteorological mast and sonic anemometer measurements, (b) wind direction measured at *R/V Polarstern* at the height of 37 m, (c) 2-m air temperature measured at the meteorological mast, (d) temperature difference between the snow surface and 2 m air, and (e) relative humidity measured at the meteorological mast at the height of 1.7–4.8 m.

to define the turbulent fluxes and stability parameters. The sensible heat flux H was calculated by the eddy correlation method

$$H = -\rho c_p \overline{\theta' w'} \quad (1)$$

where $\overline{\theta' w'}$ is the covariance of the turbulent fluctuations of potential temperature (θ') and vertical wind velocity (w'), ρ is the air density, and c_p is the specific heat.

[13] The vertical profiles of the wind speed and air temperature were measured using a 10-m-high mast with Aanderaa cup anemometers at five levels and air temperature sensors at three levels (Table 2). The relative humidity and wind direction were measured at one level. The breakup of the ISPOL floe on 24–25 December resulted in damage to the profile mast. The mast had to be moved from Site I to III and shortened to 6.5 m, with wind speed and air temperature sensors at three levels and relative humidity at one level. The wind and temperature sensors were calibrated in a laboratory

Table 2. Sensor Heights on the Meteorological Masts

Measurement Quantity	Sensor Type	Heights on the 10-m Mast (m)	Heights on the 6.5-m Mast (m)
Wind Gust	cup anemometer	10.21	6.40
Wind Direction	wind vane	10.21	6.40
Wind Speed	cup anemometer	10.21, 4.86, 2.31, 1.16, 0.55	6.40, 1.79, 0.55
Air Temperature	platinum sensor	10.16, 2.26, 0.50	6.35, 1.74, 0.50
Relative Humidity	capacitive polymer	4.81	1.74

before the experiment, but this could not be repeated after the mast failure and replacement of the sensors. The moisture sensor was compared in the field against an aspirated psychrometer and the moisture sensors of RV Polarstern and the AWI team. On the basis of these comparisons, the relative humidity was accurate within ±2 to 3% (±5% during the coldest nights).

2.4. Calculation of the Latent Heat Flux

[14] Since the water vapor flux was not directly measured, it was calculated by the bulk aerodynamic method as

$$E = \rho C_{EZ}(q_Z - q_S)V_Z \tag{2}$$

where V is the wind speed and q is the specific humidity. The subscript s refers to the surface and z to the height in the air. The latent heat flux (£E) is obtained by multiplying E by the latent heat of evaporation (£). The turbulent transfer coefficient C_E depends on the surface properties and thermal stratification. Based on the Monin-Obukhov similarity theory, the transfer coefficient for water vapor is defined as [e.g., *Launiainen*, 1995]

$$C_{EZ} = \frac{k^2}{[\log(z/z_0) - \psi_M(z/L)][\log(z/z_q) - \psi_E(z/L)]} \tag{3}$$

where z_0 and z_q are the roughness lengths for momentum and moisture, respectively. Ψ_M and Ψ_E are empirical functions describing the effect of atmospheric stratification on turbulent exchange, with the Obukhov length L as a scale parameter. For the unstable region, we applied *Högström*'s [1988] forms, while for the stable region we used those by *Holtslag and De Bruin* [1988]. In practice, the solution of equations (2) and (3) requires iteration using wind and temperature gradients from the meteorological mast. It was done by the algorithm of *Launiainen and Vihma* [1990]. The iteration yields z_0 but not z_q, because we had moisture observations from a single level only. The z_q was therefore calculated following *Andreas* [1987]. During the observation period, $C_{E3.5m}$ was $(1.9 \pm 0.4) \times 10^{-3}$ (mean ± standard deviation), yielding $(1.6 \pm 0.3) \times 10^{-3}$ for C_{E10m}, which is typical for snow-covered sea ice.

[15] For comparison against results based on equation (1), also the sensible heat flux was calculated on the basis of a bulk method analogous to equation (2). Based on the comparisons, the uncertainty in the sensible heat flux is ±5 W m^{-2}. On the basis of sensitivity tests applying the flux profile scheme of *Launiainen and Vihma* [1990], the uncertainty in the latent heat flux is also ±5 W m^{-2}.

2.5. Snow Surface Temperature

[16] As the snow surface specific humidity q_S depends solely on temperature, an accurate surface temperature is crucial in equation (2). Measurement of the snow surface (skin) temperature is difficult in the presence of intense solar radiation, which causes errors in measurements using temperature probes. In practice, the surface temperature can be best measured by radiative methods. The snow surface temperature T_S was calculated from the corrected longwave radiation data

$$T_s = \left(\frac{Lw_{out} - (1-\varepsilon)Lw_{in}}{\varepsilon\sigma}\right)^{1/4} \tag{4}$$

where σ is the Stefan-Boltzmann constant (5.67×10^{-8} W m^{-2}K^{-4}), and ε is the surface emissivity (we used $\varepsilon = 0.98$). The surface albedo for longwave radiation is assumed to be $1 - \varepsilon$.

[17] The surface temperature was also calculated from the profile mast and sensible heat flux observations applying the Monin-Obukhov similarity theory

$$T_s = T_z + 0.01z - \frac{H(\ln z/z_0 - \Psi_M(z/L))(\ln z/z_T - \Psi_H(z/L))}{\rho c_p k^2 V_z} \tag{5}$$

where z_T is the roughness length for heat, derived from the measurements, and $\Psi_H = \Psi_E$. Comparison of the fully independent surface temperatures based on equations (4) and (5) is presented in Figure 3. The maximum differences reach 0.8°C, and the maximum values of the radiation-based T_S reach 0.7°C in melting conditions, while in reality T_S of snow cannot exceed 0°C. Hence, we conclude that the accuracy of our surface temperature data is ±0.8°C, which corresponds to ±4 W m^{-2} in outgoing longwave radiation. Because of the similar pyrgeometers used and the same factor (dome heating) as an identified error source, we assume that also the accuracy of the incoming longwave radiation is ±4 W m^{-2}.

3. Time Series of Radiative and Turbulent Surface Fluxes

3.1. Shortwave and Longwave Radiation

[18] The time series of incoming and net shortwave radiation are presented in Figures 4a and 4b. The highest incoming shortwave radiation exceeded 900 W m^{-2}, and even during cloudy days the maxima were 400–600 W m^{-2}. No seasonal trend is visible in the time series, as the measurement period was around the summer solstice and changes in the cloud cover dominated the variations.

[19] The atmospheric transmissivity for shortwave radiation was calculated as the ratio of the incident shortwave radiation at the top of the atmosphere (depends on the solar zenith angle) and the observed incoming radiation at the snow surface. The results (Figure 4c) show values ranging from 0.2 to 1.1. The variability is mostly related to changes in the cloud cover but also to the diurnal cycle of the optical path

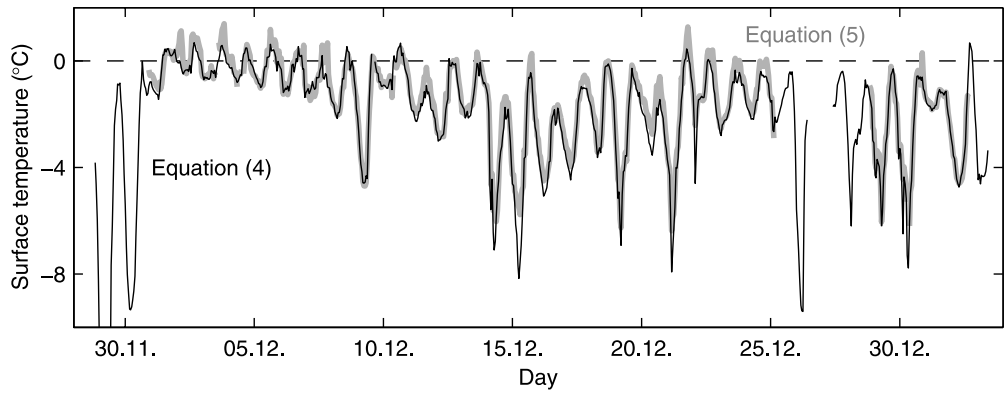

Figure 3. Snow/ice surface temperature derived from the measured longwave radiation (equation (4), black line) and the estimate based on the Monin-Obukhov similarity theory (equation (5), gray line).

of the solar beam (section 4). Values exceeding unity are possible under partly cloudy skies when the clouds do not obscure the direct solar beam and there are simultaneously strong multiple reflections between the cloud base and the snow surface.

[20] As albedo measurements are not reliable under large solar zenith angles and low flux magnitudes, results on surface albedo are only shown for solar zenith angles less than 80° (Figure 4d). Other gaps in the time series are due to relocation of the instruments (Table 1) or the presence of frost, snow flakes, or condensed water on the pyranometer domes. The albedo shows a decreasing trend from 1 to 16 December at Site I, from 21 to 26 December at Sites I and II, and from 27 December to 2 January at Site III. From 15 to 21 December the albedo had a temporary increasing trend. It was caused by snow fall and drifting snow related to a passage of a low-pressure system with stronger winds. The sudden increase in albedo between 26 and 27 December was caused by snow fall and relocation of the equipment from Site II to III. The overall change in albedo was small: only from 0.9 to 0.8 in 26 days (1–26 December). This was related to the small amount of energy available for snowmelt (section 3.3). From 17 to 25 December the time series of the albedo at Sites I and II overlap. The values, however, differ only slightly from each other, although the snow surface was visually different in the two places, being more compact with larger crystals at Site II. Also, the snow thickness was different (mean values 0.6 and 0.15 m for Sites I and II, respectively), but usually the albedo starts to significantly decrease only when the snow thickness drops below 0.1 m [*Grenfell and Perovich*, 2004; *Pirazzini et al.*, 2006].

[21] The variations in the outgoing longwave radiation emitted by the snow surface were small (Figure 5), and followed the variations in the surface temperature. The incoming longwave radiation increased during cloudy days and warm atmosphere, and was much more variable than the outgoing one. The net longwave radiation ($Lw_{net} = Lw_{in} - Lw_{out}$) was negative throughout the measurement period. Under cloudy skies it was typically -20 to -5 W m^{-2}, and -100 to -80 W m^{-2} under clear skies.

[22] The correlation coefficient (r) between the incoming shortwave radiation and the air temperature was low (0.18), while it was higher (0.41) between the incoming shortwave radiation and the surface temperature (Figure 6). Both air and surface temperature were more strongly related to the incoming longwave radiation: r = 0.65 for the air temperature and r = 0.61 for the surface temperature. Under large radiative fluxes (either shortwave or longwave), the surface temperature was always close to 0°C. In the case of smaller fluxes, the surface temperature showed a lot of variability. Its minimum value for a certain radiative flux had, however, a strong linear dependence on the incoming radiation (Figures 6e and 6f): r = 0.95 both for the shortwave and longwave radiation. The linear relationships are as follows

$$T_{S,\min} = 0.0085 \times Sw_{in} - 10.5 \quad (6)$$

$$T_{S,\min} = 0.0788 \times Lw_{in} - 26.5 \quad (7)$$

where Sw_{in} and Lw_{in} are in W m^{-2} and $T_{S,min}$ is in °C. We propose the following explanation for the high correlations. Under a certain shortwave radiation, the minimum surface temperature was obtained when the incoming longwave radiation was small, and the turbulent fluxes transported heat from the surface to the atmosphere. This was typically the case under (almost) clear skies, and the minimum surface temperature was controlled by the incoming shortwave radiation, resulting in equation (6). At nighttime, the incoming shortwave radiation was very close to zero (Figure 4) and the turbulent fluxes were also very small (section 4). The surface temperature was therefore controlled by the incoming longwave radiation, resulting in equation (7). The coefficients of equation (6) are only valid in conditions resembling the ISPOL period: the incoming clear-sky longwave radiation and the turbulent fluxes are different in other seasons and climate zones. Equation (7) may, however, be applicable in a wider range of conditions, as long as the net solar radiation and the turbulent fluxes are close to zero at nighttime.

3.2. Sensible and Latent Heat Fluxes

[23] The sensible heat flux (Figure 7a) was most of the time negative, i.e., directed from the snow surface to the air. During the calm and warm period from 1 to 13 December, the sensible heat flux had a small magnitude (on average -4 W m^{-2}), but it later increased so that the mean value over the measurement period was -6 W m^{-2}. In most nights the

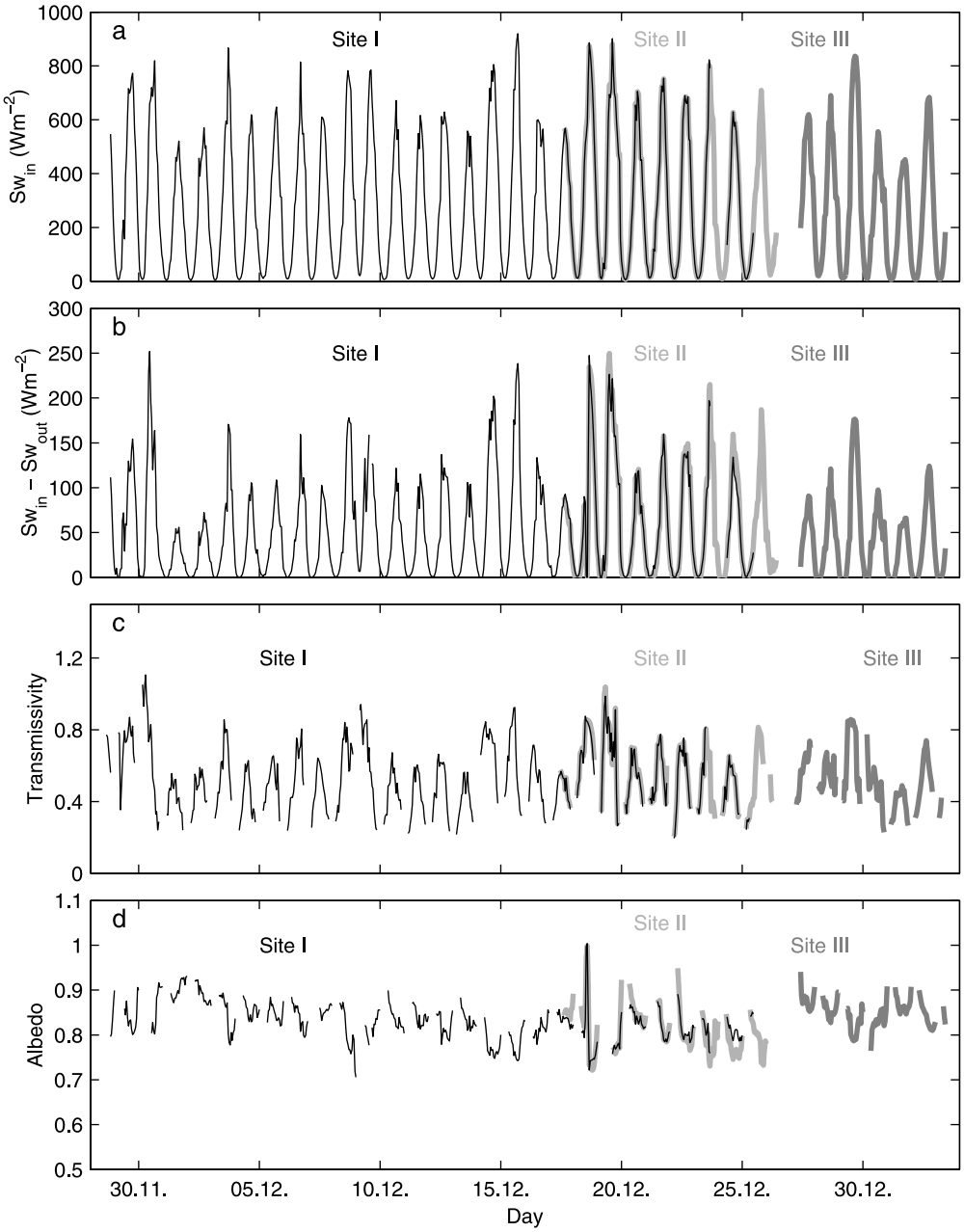

Figure 4. Time series of (a) incoming shortwave radiation, (b) net shortwave radiation, (c) atmospheric transmissivity for shortwave radiation, and (d) surface albedo for solar zenith angles less than 80°.

flux was zero or turned slightly positive, but remained negative through two nights.

[24] The maximum magnitude of the sensible heat flux exceeded 50 W m^{-2}, which is a rare value over sea ice. This occurred on 14 December, and can be explained by cold air advection from the south-southeast. We calculated the heat advection on the basis of the ECMWF operational analyses: the cold air advection at the 1000 hPa level was 5 K day^{-1}, which is close to the observed decrease of 6 K in the 2-m air temperature (Figure 2). The minimum air temperature was reached at noon solar time. Also, the snow surface temperature decreased, but the noon value was only 2°C lower than in the two preceding days (Figure 3). This was due to the intensive solar heating (Figure 4) and the fact that an almost isothermal wet layer with temperature at 0°C was close below (Nicolaus et al., submitted manuscript, 2009), providing an effective buffer against snow temperature variations (the observed surface temperature changes were only representative for a thin skin layer). Hence, the conditions favored development of a large surface air temperature difference in the afternoon of 14 December: the minimum (i.e., maximum upward) sensible heat flux coincided with the minimum air temperature. On 15 and 16 December, the ECMWF analyses did no more show clear signs of cold air advection, and the daytime minima in the sensible heat flux increased (Figure 7). All cases with $H < -20$ W m^{-2} occurred approximately at noon; the incoming solar radiation had a more direct effect on the snow surface than air temperature (Figure 6). The cases

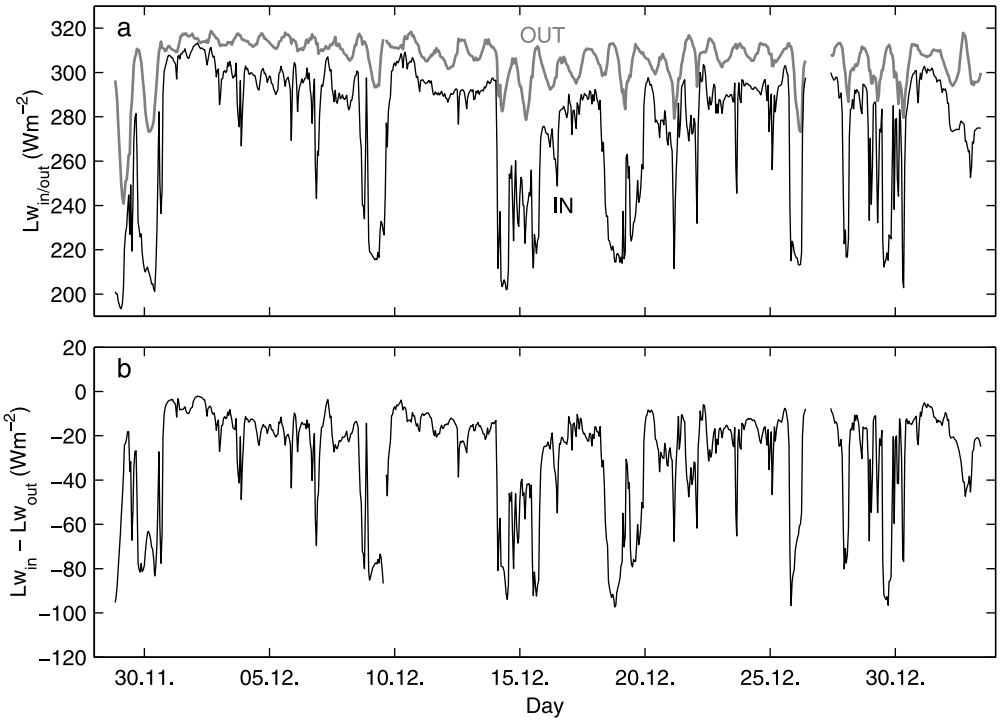

Figure 5. Time series of (a) outgoing and incoming longwave radiation and (b) net longwave radiation.

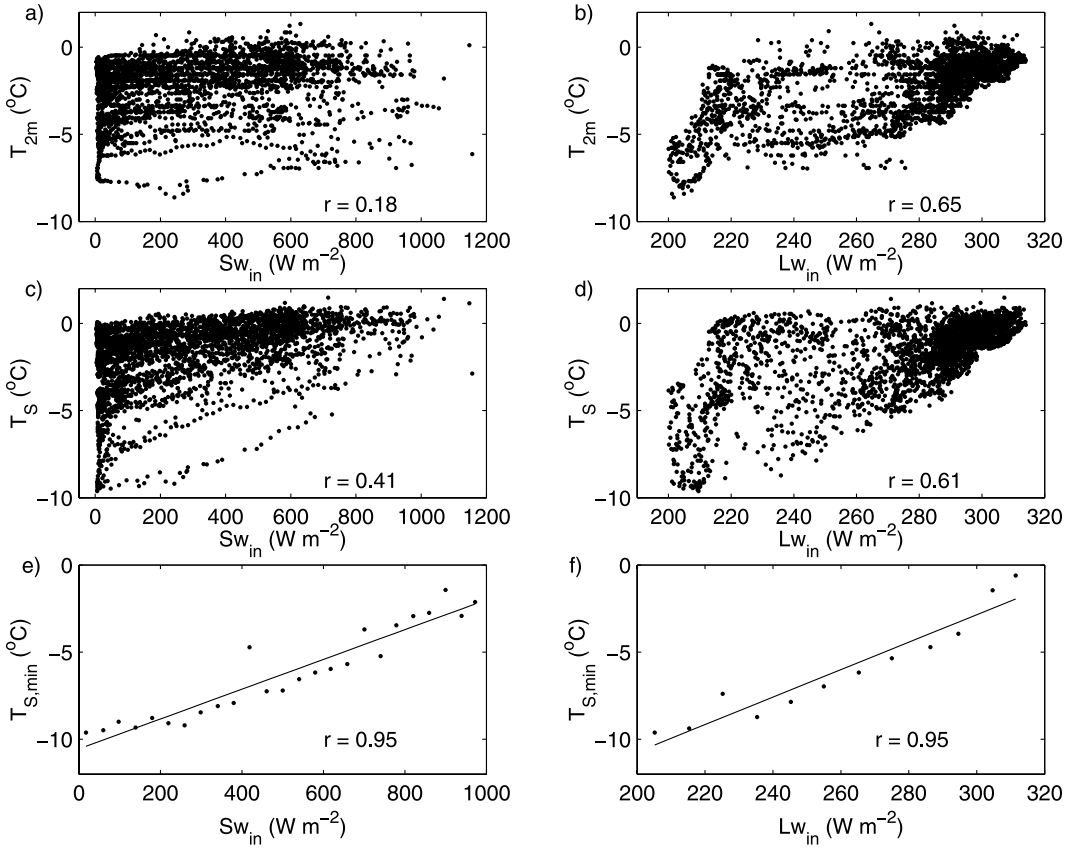

Figure 6. Dependence of (a and b) the 2-m air temperature and (c and d) the snow surface temperature on the incoming shortwave (Sw_{in}) and longwave (Lw_{in}) radiation. Dependence of the minimum snow surface temperature on the incoming (e) shortwave and (f) longwave radiation.

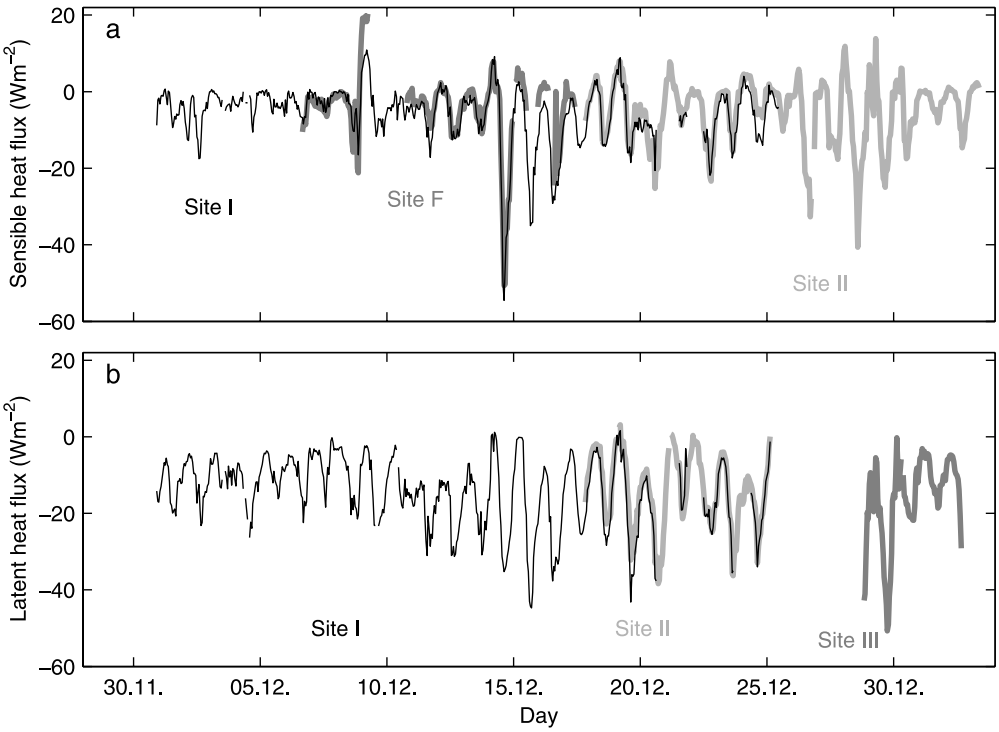

Figure 7. Surface fluxes of (a) sensible heat based on the sonic anemometer measurements and (b) latent heat calculated using the Monin-Obukhov similarity theory.

with downward sensible heat flux were not related to warm air advection, but all occurred in nighttime due to a negative radiation balance.

[25] The spatial differences in the sensible heat flux within the ISPOL floe remained small compared to the temporal variations. This was revealed by comparing simultaneous data from the two measurement sites (I and II) from 17 to 25 December (Figure 7). The root mean square difference between the fluxes at the two sites was 3 W m^{-2}. In addition, the sensible heat flux measured on 6 to 17 December at Site F compares well with that at Site I on the ISPOL floe (Figure 7a), although the former was on a larger, thicker, and rougher floe.

[26] Also, the latent heat flux was mainly directed from the snow surface to air, and most of the time it had a larger magnitude than the sensible heat flux. The latent heat flux also had a decreasing trend and an increasing diurnal amplitude (Figure 7b). The former was related to a decrease in the air relative humidity, and the latter to a decrease in the cloud cover. The mean latent heat flux over the study period was −14 W m^{-2}. The Bowen ratio (Bo = H/£E) was 0.3 ± 1.6.

[27] To better understand the factors controlling the turbulent fluxes, we applied the METEX program [*Zeng et al.*, 2003] to search the backward trajectories for the air masses observed at ISPOL: 72-h backward trajectories were calculated once a day. The results indicated that in 50% of the cases the air mass had crossed the Antarctic Peninsula, while in 25% of the cases it had originated from the ice-covered Weddell Sea, and in 25% of the cases from the open ocean in the north or northeast. During periods with the origin in the open ocean, as 2–8 December, the turbulent fluxes had a small magnitude and diurnal cycle (Figure 7). Having crossed the Antarctic Peninsula (9–11, 13–14, 16, 18, and 27–31 December and 1–2 January) the air mass was usually drier and the fluxes had a larger magnitude and diurnal cycle.

3.3. Net Heat Flux and Snow Thinning

[28] The net heat flux from the Sun and atmosphere to the snowpack (Q_{net}) was calculated as

$$Q_{net} = Sw_{net} + Lw_{net} + H + £\mathrm{E} \tag{8}$$

where Sw_{net} and Lw_{net} are the shortwave and longwave net radiation, respectively. Time series of the net heat flux are shown in Figure 8: the mean value is 3 W m^{-2}. It should be noted that Q_{net} does not equal the net heat flux at the snow surface, as the conductive heat flux from the snowpack is not included. The mean snow surface temperature was −2.1°C, and the ice bottom temperature kept at the freezing point of −1.8°C, but an almost isothermal (0°C) layer of wet snow existed in between (Nicolaus et al., submitted manuscript, 2009). Hence, the conductive heat flux was not negligible, and will be addressed in section 4.

[29] The inaccuracies of the components of Q_{net} are 4 W m^{-2} (1–2%) for both incoming and outgoing longwave radiation, 8 W m^{-2} (3%) for both incoming and reflected shortwave radiation, and 5 W m^{-2} (30–90%) for the sensible and latent heat fluxes. If the errors remaining in the longwave radiation still after the calibration correction are mostly due to the dome heating effect (which under a high albedo is almost the same for the upward- and downward-looking pyrgeometer), we can assume that the errors in the incoming and outgoing components tend to cancel each other in $\mathrm{Lw_{net}}$. Hence, the relative inaccuracy in $\mathrm{Lw_{net}}$ is approximately the same as in its components (1–2 %), yielding 1 W m^{-2} for the error of the net longwave radiation ($\mathrm{E_{Lw-net}}$). Errors in

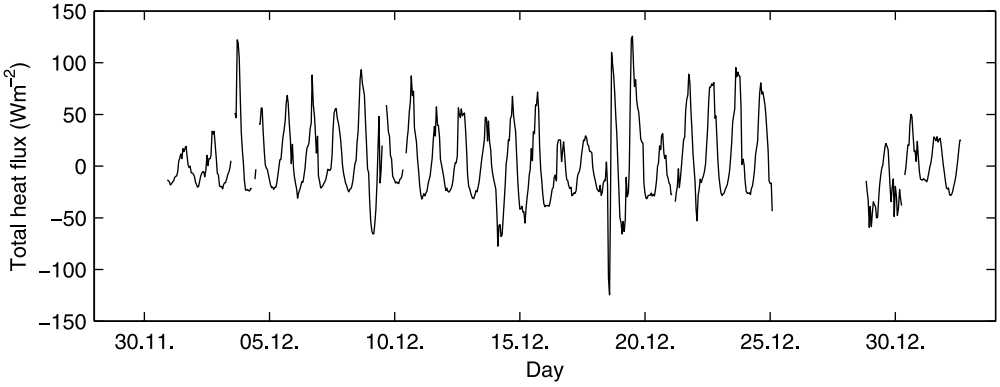

Figure 8. Time series of the net radiative and turbulent surface heat flux Q_{net}.

the incoming and reflected shortwave radiation are probably mostly related to the magnitude of the incoming radiation (as the albedo was high and fairly constant), and therefore tend to cancel each other [*Schmidt and König-Langlo*, 1994]. Hence, the error in the net shortwave radiation (E_{Sw-net}) should only be 2 W m^{-2}. Finally, the errors in the fluxes of sensible (E_H) and latent heat (E_{LE}) are independent of each other and most likely of the errors in the radiative fluxes. Following the assumption of dome heating as the main source for the error in the longwave radiation, $E_{Lw\text{-}net}$ and $E_{Sw\text{-}net}$ depend on each other. Hence the error in the net heat flux (E_{net}) can be estimated as

$$E_{net} = \sqrt{E_H^2 + E_{LE}^2 + (E_{Sw-net} + E_{Lw-net})^2} \qquad (9)$$

which yields 8 W m^{-2}. It is, however, not clear what are the reasons for the errors remaining in the longwave radiation after the calibration correction (see *Kohsiek et al.* [2007] for various error sources). The maximum estimate for E_{net} is obtained by assuming that the errors in the incoming and outgoing components are entirely independent of each other, which yields 6 W m^{-2} for E_{Lw-net}, but dependent on E_{Sw-net}. Then equation (9) yields 11 W m^{-2} for E_{net}.

[30] Considering the error of the average Q_{net} over the measurement period ($\overline{E}_{\mathrm{net}}$), we first studied the autocorrelation timescale of the successive flux observations. For timescales of 24 h and longer, the autocorrelation was no more statistically significant. Accordingly, assuming that the errors in the components of Q_{net} were random errors, we get $\overline{E}_{net} = E_{net}/\sqrt{n}$, where n is the number of 24 h periods, yielding ±1 or ±2 W m^{-2} for $\overline{E}_{\mathrm{net}}$ depending on the calculation of E_{net} (8 or 11 W m^{-2}). Accordingly, we can conclude that during ISPOL there was a slight net downward heat flux to the snowpack.

[31] Despite of 0.08 m of snow accumulation, the observed snow thinning during ISPOL was 0.1 to 0.2 m [*Haas et al.*, 2008]. Our observations indicated an increase of snow density from 300 to 350 ± 30 kg m^{-3} through the snowpack at Site I. Using 0.5 ± 0.1 m as an initial snow thickness, the increase in density at Site I yields snow thinning of 0.09 ± 0.06 m during the study period. Accordingly, we should find factors responsible for additional 0.03 to 0.25 m of snow thinning. With our mean latent heat flux of −14 ± 5 W m^{-2} and a snow density of 330 kg m^{-3}, the snow thinning due to evaporation was 0.05 ± 0.02 m in 34 days. Our result for the net heat flux to the snowpack was (3 ± 2) W m^{-2}. Part of the net surface heat flux observed was, however, used for rising the snow and ice temperatures toward the melting point. The observed increase in snow temperature ranged from 0.1 to 1.9°C [*Haas et al.*, 2008], which in 34 days required (0.1 ± 0.1) W m^{-2}. *Haas et al.* [2008] further observed a mean increase of 0.9 K in the temperature of 1.5-m-thick sea ice (their Figure 9), which according to our calculations has required 1.8 W m^{-2}. Without thermodynamic air-ice-ocean model experiments, it is, however, impossible to solve how large portions of the heat originated from above and below the ice. The mean oceanic heat flux at the ice bottom was 15 W m^{-2} [*McPhee*, 2008], i.e., five times larger than the net flux at the snow surface, but the results of *Haas et al.* [2008, their Figure 9] indicate maximum warming in the upper parts of the sea ice cover. Hence without including the warming of sea ice in the calculations, we give the maximum estimate for the heat available for melting: 2.9 ± 2 W m^{-2}, which can explain approximately 0.08 ± 0.05 m of snow thinning. With the above mentioned error margins, we estimate that the contributions of the increase in snow density, melt, and evaporation were approximately equally important for the observed snow thinning.

4. Diurnal Cycles

[32] The mean diurnal cycles in various quantities are presented in Figure 9. Both incoming and reflected solar radiation had a clear cycle with amplitudes of 320 and 260 W m^{-2}, respectively. The atmospheric transmissivity for shortwave radiation naturally had a strong diurnal cycle because the optical path of the solar beam depends on the zenith angle. Slightly lower values in the afternoon than morning cannot be explained by the diurnal distribution of cloud occurrence, based on ceilometer and visual observations, but the asymmetry is supposed to be related to differences in cloud properties.

[33] Reliable detection of the diurnal cycle of albedo requires very accurate observations. Hence only the Eppley PSP pyranometer data from Site I were applied. The diurnal amplitude of the surface albedo was on average 0.02 (Figure 9c). In the days when surface melting occurred for at least 2 hours, the diurnal cycle was larger with a mean amplitude of 0.04. The albedo decreased through the morning, and the minimum values were observed from 13 to 19 local solar time (LST) (reliable values cannot be calculated

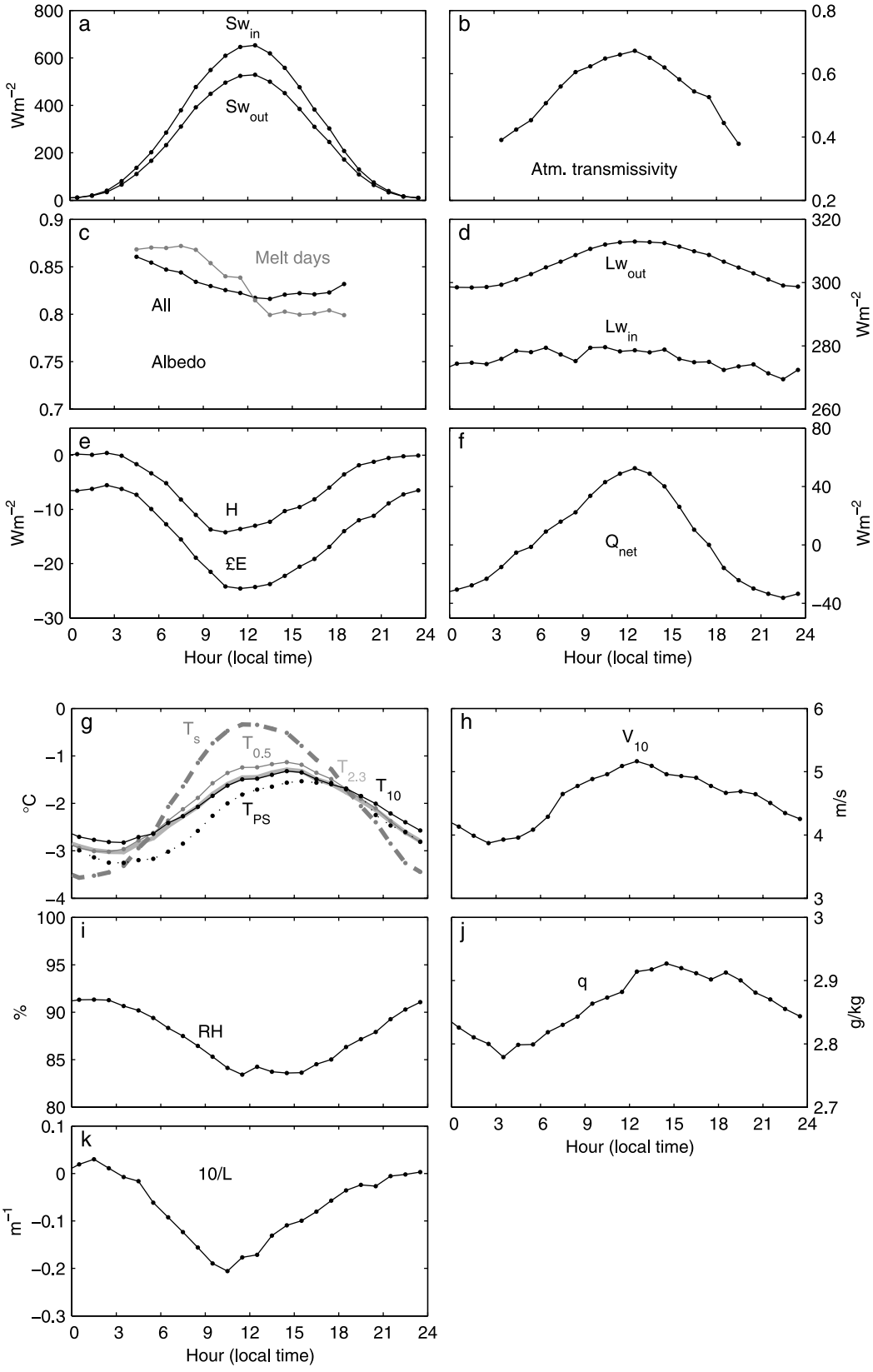
a
Sw_in
Sw_out
Wm^-2
b
Atm. transmissivity
c
Melt days
All
Albedo
d
Lw_out
Lw_in
Wm^-2
e
H
£E
Wm^-2
f
Q_net
Wm^-2
Hour (local time)
Hour (local time)
g
T_s
T_0.5
T_2.3
T_10
T_PS
°C
h
V_10
m/s
i
RH
%
j
q
g/kg
Hour (local time)
k
10/L
m^-1
Hour (local time)

Figure 9

for solar zenith angles larger than 80°). The diurnal cycle was asymmetric, which probably resulted from the compensating effects of the solar zenith angle and snow metamorphosis. The dependence of albedo on solar zenith angle should generate a U-shaped diurnal cycle, but in the afternoon the snow crystals are rounded by melting and transport of water vapor inside the snowpack. The afternoon cooling of the snowpack below the surface takes place via heat conduction, which is much slower process than radiative heating. Hence crystals remain rounded still late in the afternoon. These processes tend to decrease the albedo compensating the effect of the solar zenith angle [*Pirazzini*, 2004]. In the melt days the morning albedo was higher than in the population of all days. This was because melt days were more frequent in the early part of the study period (Figure 2c), when the daily mean albedo was still higher (Figure 4d).

[34] The outgoing longwave radiation had a sinusoidal diurnal cycle (Figure 9d; amplitude 7 W m^{-2}), originating from the cycle in the surface temperature. The diurnal cycle of the incoming longwave radiation (amplitude 5 W m^{-2}) was somewhat disturbed by synoptic-scale changes in the cloud cover, which occurred mostly randomly with respect to the time of the day (except for the lowest clouds; see below).

[35] The turbulent fluxes of sensible and latent heat both had an apparent sinusoidal cycle with diurnal amplitudes of 7 and 10 W m^{-2}, respectively (Figure 9e). The diurnal amplitudes of the sensible and latent heat fluxes and the outgoing longwave radiation only represent 2–3% of the diurnal amplitude of 320 W m^{-2} of the incoming solar radiation. For the turbulent heat fluxes, the maximum magnitudes were obtained around 10–11 LST (sensible heat) and 10–13 LST (latent heat), while for the outgoing longwave radiation the maximum magnitudes occurred around 11–14 LST. The earlier maximum magnitudes for the turbulent heat fluxes were due to the fact that in the morning the surface temperature increased faster than the air temperature. During the calm and warm period from 1 to 13 December, the sensible heat flux and its diurnal variation were small. The stability parameter 10/L (median values in Figure 9k) reached its minimum value at 10–11 simultaneously with the minimum sensible heat flux. Even the daytime values of 10/L only indicate slightly unstable stratification. From 23 to 03 LST, the median 10/L indicated slightly stable stratification.

[36] The net heat flux available to heat or melt the snowpack was calculated as a residual of the radiative and turbulent surface fluxes (Figure 9f). Around noon the net heat flux to the snowpack exceeds 50 W m^{-2}, while in nighttime the snowpack releases almost 40 W m^{-2}. Averaged over the study period, the observations demonstrate that at night hours (approximately from 20 to 03 local time) there was practically no temperature difference between the heights of 0.5 and 2.3 m in the air (the lines merge in Figure 9g), and the mean sensible heat flux measured at the height of 3.5 m was close to zero (Figure 9e). The surface temperature was, however, up to 0.7 K lower than the 0.5-m air temperature. A few cases with a large temperature difference were important in generating this mean difference, and we interpret the cases as follows. In nighttime conditions the snow surface cools due to the negative radiation balance and, if the wind is weak, the surface becomes thermally decoupled from the air at a few meters height: the surface sensible heat flux approaches zero, while the temperature gradient increases. This is a well-known feature in a stable boundary layer [*Mahrt*, 2002], also over sea ice [*Grachev et al.*, 2005]. The measurements at the height of 3.5 m do not necessarily represent the true surface flux, but previous studies of similar conditions have demonstrated that decoupling is only possible, if the surface flux is very close to zero [*van de Wiel et al.*, 2007].

[37] The snow surface temperature had a mean diurnal amplitude of 1.6°C with the maximum values reached between 11 and 13 LST (Figure 9g). Surface melting for at least 1 hour occurred on 16 days, but it only slightly reduced the diurnal temperature cycle. The air temperature had a clear diurnal cycle: at the heights of 0.5, 2.3, and 10 m the diurnal amplitude was 0.9, 0.9, and 0.8°C, respectively, which correspond to 47–58% of the amplitude of the surface temperature. Due to the prevailing unstable stratification, the amplitude was not particularly sensitive to the observation height. A long delay in the temperature rise in the morning was observed at *R/V Polarstern* at the height of 27 m and the amplitude (0.9°C) was higher than at the height of 10 m, which are probably due to disturbances generated by the ship. A very shallow super adiabatic surface layer was generated during daytime, seen as a clear difference between the temperatures at the heights of 0.5 and 2.3 m (Figure 9g). Between the heights of 2.3 and 10 m the mean profile was, however, merely adiabatic. In cases of stable surface-layer stratification during night, the diurnal cycle was much stronger and the amplitude depended much more on the observation height, e.g., on 15 December the amplitude was 2.0°C at the height of 0.5 m and 1.1°C at the height of 10 m, and, due to the decoupling, 3.9°C at the snow surface (Figure 3).

[38] The 10-m wind speed (Figure 9h) showed a sinusoidal diurnal cycle with an amplitude of 0.6 m/s and maximum values around noon, when the surface-layer stratification was most unstable. The minimum values occurred at night when the stratification was usually near-neutral or stable. Assuming that the large-scale pressure gradient did not have any systematic diurnal cycle, the results can be explained by the enhanced vertical turbulent transport of momentum during the daytime convective conditions, which results in stronger near-surface winds.

[39] The specific humidity at the height of 4.8 m had a weak diurnal cycle (amplitude 0.07 g/kg) with maximum

Figure 9. Mean diurnal cycles of (a) incoming and outgoing shortwave radiation, (b) atmospheric transmissivity for shortwave radiation, (c) surface albedo for all observation days and for days with at least 2 h of surface melting, (d) incoming and outgoing longwave radiation, (e) surface fluxes of sensible and latent heat, (f) net heat flux for heating and melting of the snow, (g) snow surface temperature and the air temperature at the heights of 0.5, 2.3, and 10 m at the meteorological mast and 27 m at *R/V Polarstern* (T_{PS}), (h) 10-m wind speed, (i) air relative humidity, (j) air specific humidity, and (k) stability parameter 10/L. The cycles are calculated on the basis on mean values for each hourly interval, except that median values are applied for 10/L, because it has a strongly nonlinear dependence on the surface fluxes.

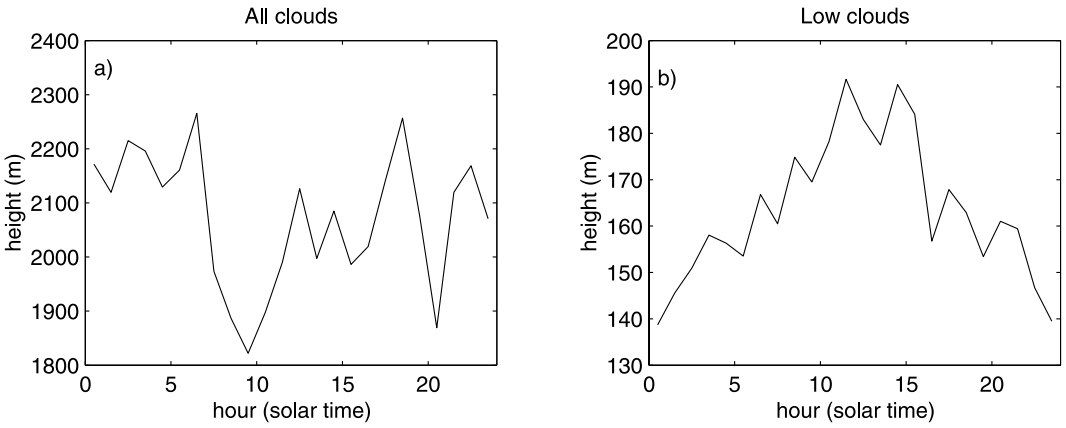

Figure 10. Mean diurnal cycle of the cloud base for (a) all clouds and (b) clouds with the base height lower than 300 m.

values in the afternoon. The diurnal cycle of the relative humidity (amplitude 4%) was, however, opposite to that of the specific humidity, and dominated by the air temperature: the minimum relative humidity was observed in the afternoon simultaneously with the highest air temperature.

[40] The diurnal cycle of the cloud base height was studied on the basis of *R/V Polarstern* ceilometer data. Including all clouds in the analyses, no clear diurnal cycle was found, although the values were generally lower during daytime, particularly between 7 and 11 LST (Figure 10a). For clouds with the base height lower than 300 m, a clear diurnal cycle was, however, detected (Figure 10b). The cloud base was highest around noon, and the diurnal amplitude was 26 m. For these seemingly contradicting results we suggest the following explanation: the morning solar heating and unstable stratification resulted in local formation of convective clouds, which have much lower base heights than clouds advected over the Weddell Sea. The number of cases with low clouds detected was indeed highest from 8 to 10 LST (with an equal maximum from 3 to 4 LST) coinciding with the minimum cloud base for all clouds. Between 18 and 19 LST the number of cases with low clouds was only 68% of its morning value. Yet only focusing on cases with low clouds present (Figure 10b), the base height rises during the daytime convection and warming.

5. Discussion

5.1. Processes in the Antarctic Sea Ice Zone

[41] The ISPOL measurements by *Nicolaus et al.* [2006] yielded albedo values ranging from 0.85 to 0.67. Most of the time the difference between their and our values was approximately 0.03 only; it may have arisen from small-scale spatial differences and measurement inaccuracies. In any case, the decrease of albedo during the 34-day period was not enough to trigger any significant positive feedback effect. Therefore the net heat flux and snowmelt did not show an increasing trend during the study period. Also, the results by *Brandt et al.* [2005] suggest that there is no significant albedo feedback in the Antarctic sea ice zone. They analyzed albedo data from ship-based field experiments in the East Antarctic sea ice zone, and concluded that a representative albedo of snow-covered sea ice is 0.87 in September–November and 0.82 in December–February. Also, based on ship data, *Wendler et al.* [2005] observed a mean albedo of 0.81 for compact sea ice cover in late December. Although ship-based albedo measurements are not as accurate as those made at an ice station, the numbers are very close to our mean value of 0.83 for December.

[42] Snow surface albedo is also strongly controlled by precipitation, as snow fall tends to increase albedo [*Pirazzini*, 2004]. In the Weddell Sea precipitation is less than in other areas at the same latitude because of the Antarctic Peninsula blocking humid westerly winds and depressions on its western side [*Tietäväinen and Vihma*, 2008]. Air on the east coast of the Peninsula is generally 7 K colder than at similar latitudes and elevations on the west coast. From the point of view of the summer decrease of albedo, the effects of low temperatures and reduced snow fall in the Weddell Sea tend to compensate each other, which partly explains the similarity between our observations and those made at the East Antarctic sea ice zone [*Brandt et al.*, 2005; *Wendler et al.*, 2005].

[43] In days with surface melt for at least 2 hours, the diurnal cycle of albedo observed at ISPOL was comparable to the seasonal trend through the study period. Our observations on the shape of the cycle are in agreement with results from several locations over the Antarctic continent [*Pirazzini*, 2004], but we are not aware of any previous studies on the diurnal cycle of surface albedo in the Antarctic sea ice zone. We are neither aware of previous studies on the atmospheric transmissivity for shortwave radiation over the Antarctic sea ice zone. Compared to our December mean of 0.50, *Van den Broeke et al.* [2004] observed an annual mean value of 0.63 at the Riiser-Larsen Ice Shelf and 0.78 at the Kohnen station 530 km inland from the ice shelf front at the altitude of 2900 m.

[44] Our results for the ISPOL period indicated an upward sensible heat flux. On the contrary, the prevalence of a downward sensible heat flux over Antarctic sea ice was observed by *Andreas et al.* [2000, 2004, 2005] in February–May at ISW in the same region as ISPOL, and in four studies in more eastern parts of the Weddell Sea: *Kottmeier and Engelbart* [1992] in October–November, *Launiainen and Vihma* [1994] for most of the year, and *Vihma et al.* [1996, 2002] throughout the year. It seems that the sensible heat flux over Antarctic sea ice is from air to snow for most of the year.

[45] In summer the direction of the sensible heat flux seems to be variable. *Launiainen and Vihma* [1994] observed

a mean sensible heat flux of 20 W m^{-2} in December 1990 at 66–67°S, and *Vihma et al.* [2002] obtained a similar value for December 1996 in the same region. Their study region was located 1000 km east of ISPOL, and this may be one reason for the different flux direction: the central Weddell Sea is more often affected by warm air advection from the north, which is an important factor generating downward sensible heat flux. In the pioneering studies of *Andreas* [1985] and *Andreas and Makshtas* [1985], based on ship observations in October–November 1981, the sensible heat flux was directed from air to snow during northerly winds and from snow to air during southerly winds; the difference in the flux magnitude was up to 180 W m^{-2}. *Wendler et al.* [2005] observed a downward sensible heat flux in the Ross Sea over both broken sea ice (12 W m^{-2}) and compact snow-covered sea ice in the McMurdo Sound (18 W m^{-2}). The observation periods of the work of *Wendler et al.* [2005] were, however, short: six days over the broken sea ice and four over the compact sea ice. Hence the synoptic-scale situation may have had an essential effect on the results. In any case, the above mentioned results demonstrate that observations on turbulent fluxes from the western Weddell Sea should not be generalized for the entire Antarctic sea ice zone, not even for the entire Weddell Sea.

[46] On the basis of ISPOL observations and the prevalence of dry, cold katabatic winds, *Nicolaus et al.* [2006] concluded that in summer turbulent fluxes are predominantly upward over the Antarctic sea ice zone. This may be the case in many regions, but our results indicate that upward heat fluxes can prevail even without this effect: in only 50% of time the air masses observed at ISPOL came from the Antarctic continent, and even among these cases the air mass usually originated from the west or northwest of the Antarctic Peninsula with the flow controlled by the synoptic-scale pressure gradient. On the other hand, despite of the prevailing katabatic winds at the McMurdo Sound, *Wendler et al.* [2005] observed downward sensible heat flux.

[47] Our results provide the first extensive quantification on the diurnal cycle in various meteorological quantities affecting the snow metamorphosis over the Antarctic sea ice. We observed diurnal cycles in 15 variables. A simplified picture of the causal chain is that the diurnal cycle in the incoming shortwave radiation is the driving force for the other diurnal cycles, and it most directly affects those in the reflected solar radiation and snow surface temperature. These further affect the outgoing longwave radiation, surface albedo, and the turbulent fluxes of sensible and latent heat. The diurnal cycles in the air temperature as well as the specific and relative humidity follow in this causal chain, where the variables most indirectly affected are the incoming longwave radiation and wind speed. The base height of low clouds is affected by the air temperature and moisture as well as the incoming and reflected shortwave radiation.

[48] Although the diurnal cycle is a widely studied topic, there have not been many observations reported from the Antarctic sea ice zone. Compared to ISPOL, *Wendler et al.* [2005] observed a smaller diurnal amplitude for the incoming shortwave radiation (210 W m^{-2}, estimated from their Figure 3) but a larger one for incoming longwave radiation (approximately 15 W m^{-2}). The former was due to higher latitude (78°S). Our drifting buoy data from the central Weddell Sea at 73–65°S in 1990 indicated a diurnal amplitude of 1.4°C in the 2-m air temperature in December [*Launiainen et al.*, 1991], which is slightly larger than the ISPOL result (0.9°C). The buoy data also demonstrated that in addition to season and latitude the diurnal temperature cycle strongly depended on the ice concentration: the more open water around, the smaller was the diurnal cycle. This was also demonstrated by *Niros et al.* [2002], who compared diurnal cycles over the open and ice-covered Baltic Sea and its snow-covered coasts.

5.2. Comparisons Between the Arctic and Antarctic

[49] On the basis of ISPOL observations, *Willmes et al.* [2006, 2007] concluded that there is a fundamental difference in the summer evolution of the snowpack between the Arctic and Antarctic sea ice zones. In the Antarctic, the microwave brightness temperature drops at the onset of snowmelt, although it increases in the Arctic. According to *Willmes et al.* [2006], the reason for the drop in the Antarctic is the repeated diurnal thawing and refreezing of snow, instead of complete snow wetting as in the Arctic. Our snow surface temperature data support this conclusion.

[50] *Willmes et al.* [2006, 2007] and *Nicolaus et al.* [2006] stressed the differences in snow processes between the Arctic and Antarctic, while *Andreas et al.* [2005] concluded on the basis of ISW observations that similar processes control the ABL over sea ice in both hemispheres. The statistics on temperature inversions at ISW in February–May were similar to the Arctic: the ABL was virtually always stably stratified with near-surface inversions observed in 96% of the tethersonde soundings. Should we conclude that (1) the processes in the Arctic and Antarctic are basically similar in autumn and winter but different in summer or (2) that the processes are similar in the ABL but different in the snowpack? We try to better understand this issue by comparing the ISPOL observations against two Arctic field experiments: the Surface Heat Budget of the Arctic Ocean (SHEBA) and the Swedish Arctic Ocean Expedition 2001 (AOE-2001).

[51] In June the SHEBA ice camp was at higher latitudes than ISPOL (76–77°N), but the mean incident shortwave radiation at the top of the atmosphere (504 W m^{-2}) was very close to that of ISPOL (508 W m^{-2}), although the diurnal ranges were somewhat different: 0–1008 W m^{-2} at ISPOL and 0–800 W m^{-2} at SHEBA. We calculated from the SHEBA data that in June the monthly mean net shortwave radiation was 73 W m^{-2}, the net longwave radiation −28 W m^{-2}, the latent heat flux −6 W m^{-2}, and the sensible heat flux −2 W m^{-2} (compare to Figure 20 in *Persson et al.* [2002]). In ISPOL, the mean net solar radiation was smaller (52 W m^{-2}), the net longwave radiation approximately the same (−30 W m^{-2}), while the fluxes of latent heat (−14 W m^{-2}) and sensible heat (−6 W m^{-2}) had larger magnitudes. In SHEBA, the surface albedo decreased from 0.82 to 0.63 during June, with a mean value of 0.74, while at ISPOL the mean value was 0.83. The mean values of 2-m air temperature were −2°C for ISPOL in December and −0.5°C for SHEBA in June. With colder air and higher albedo, the snowmelt is reduced and a larger portion of the solar heating of the surface is used for evaporation and sensible heat flux to the atmosphere: at ISPOL this portion was 38% compared to 11% at SHEBA, where the solar radiation was mostly used to melt the snow and ice.

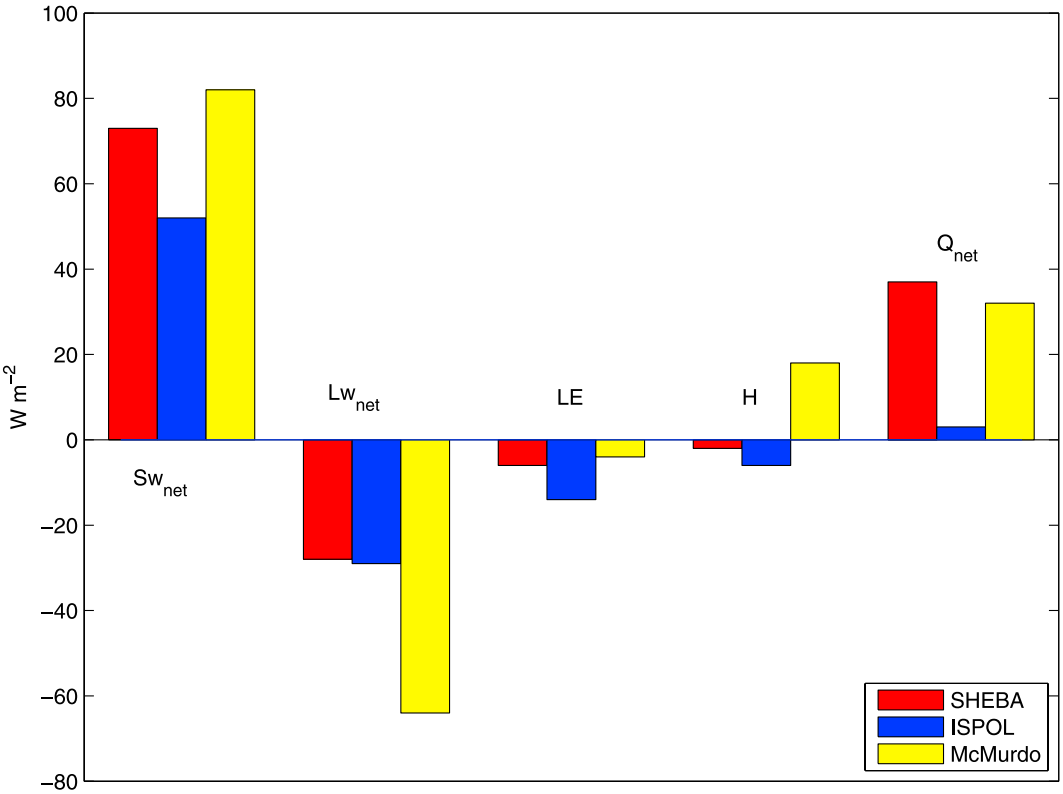

Figure 11. Mean surface fluxes at SHEBA in June 1998 (red), at ISPOL (blue), and at McMurdo Sound on 28–31 December 2000 (yellow [*Wendler et al.*, 2005, Table 3]).

[52] The difference was also seen in the maximum upward sensible heat flux, at ISPOL its magnitude exceeded 50 W m^{-2}, but was only 12 W m^{-2} in June at SHEBA. Cold air advection is an important factor generating upward sensible heat flux in polar regions [*Vihma et al.*, 2005; *Valkonen et al.*, 2008], but in summer there are not many sources of colder air to flow over the Arctic sea ice, while in the Antarctic the continent provides sources of colder air.

[53] Although the monthly mean turbulent fluxes were directed upward both at ISPOL in December and SHEBA in June, the partitioning of the incoming solar energy was different. This is illustrated in Figure 11. Although representing a short period only, the results by *Wendler et al.* [2005] from the compact sea ice cover in the McMurdo Sound are included in Figure 11 to demonstrate the variability in summer conditions in the Antarctic, which may be of spatial or temporal origin. With respect to the net shortwave and net longwave radiation as well as the sensible and latent heat flux, the ISPOL results are closer to SHEBA than the McMurdo Sound results. The residual term Q_{net} is, however, almost the same at SHEBA and McMurdo Sound, but only approximately 10% of those at ISPOL.

[54] In SHEBA in June, the incoming shortwave radiation had an amplitude of approximately 180 W m^{-2} only, while the ISPOL value was 320 W m^{-2}. Hence also other quantities had smaller diurnal cycles at SHEBA: the mean diurnal amplitudes were 0.3°C for the surface temperature, 0.6°C for the air temperature, and 3 W m^{-2} for the sensible heat flux [*Persson et al.*, 2002, Figures 16 and 17]. The ISPOL values were 1.6°C, 0.9°C and 7 W m^{-2}, respectively.

[55] In the Arctic, the diurnal cycle in the incoming shortwave radiation at the snow/ice surface is reduced after early May due to the increase in cloudiness toward summer [*Persson et al.*, 2002]. Further, the largest amplitudes of the diurnal cycles of near-surface air temperature and sensible heat flux occur even before – in April. In SHEBA, the air temperature amplitude in July (0.2°C) was already strongly reduced from the June value (0.6°C). This was related to (1) the seasonal evolution of the boundary layer stratification and (2) the onset of melt that limits the diurnal cycle in surface temperature [*Persson et al.*, 2002]. In ISPOL the surface melt was so limited that only in a few cases it notably reduced the diurnal cycle of the surface temperature (the mean cycle peaks just below 0°C; Figure 9), but at SHEBA the diurnal amplitude in June was only 20% of that at ISPOL in December.

[56] On the basis of AOE-2001 observations, *Tjernström* [2005, 2007] showed that a diurnal cycle is present over sea ice in summer even very close to the North Pole (most of his data originated from an ice drift station at 88–89°N, from 2 to 21 August 2001). In addition to the incoming shortwave and net radiation, a diurnal cycle was apparent in the wind speed, cloud base, and visibility. Due to the high latitudes, the mean amplitudes observed by *Tjernström* [2005, 2007] were naturally much smaller than at ISPOL: approximately 25 W m^{-2} in incoming solar radiation and 5 W m^{-2} in net radiation. Due to melting and refreezing, the diurnal cycle in the near-surface air temperature remained weak. *Tjernström* [2005, 2007] observed, however, a significant diurnal cycle in the wind speed with the lowest winds around noon. This is opposite to the ISPOL results. In his case the diurnal cycle

in the surface sensible heat flux was qualitatively similar to that at ISPOL with the peak value at noon, but the amplitude was much smaller. Hence there must have been some other factor that has dominated over the stratification effect and thus prevented the generation of maximum winds around noon.

[57] *Tjernström* [2005, 2007] observed a consistently high cloud fraction but slightly lower values in the morning and during late night. The cloud base height was on average lowest from 10 to 15 LST, which is approximately in agreement with the ISPOL results (Figure 10a). *Tjernström* [2005, 2007] did not make separate calculations for low clouds (as in our Figure 10b), and interpreted that the noon minimum in the cloud base height was due to complex interactions in the subcloud and cloud layers involving changes in stratification, cloud top radiative cooling, turbulent mixing, and drizzle. We think that at ISPOL, with a larger diurnal cycle in the surface temperature, the daytime heating and convection were probably enough to explain the noon maximum in the base height of low clouds, although various other processes were naturally also active in the cloud layer.

[58] In the ice-covered Baltic Sea at the latitudes of 63–64°N in February and early March 1998, *Brümmer et al.* [2002] observed air temperatures and latent heat fluxes comparable to those at ISPOL, but the sensible heat flux was predominantly from air to ice. This was often due to warm air advection over the sea ice. Its dominating effect was probably related to the small distance from the open sea, which was 0–150 km compared to 220–500 km at ISPOL. Nicolaus et al. (submitted manuscript, 2009) observed stronger snowmelting and superimposed ice formation on ice floes 100 km north of ISPOL, which demonstrates how sensitive the effects of warm air advection are to the fetch over the ice [see also *Tisler et al.*, 2008].

6. Conclusions

[59] The radiative and turbulent surface fluxes observed at ISPOL only generated a small mean net flux of (3 ± 2) W m^{-2} to the snowpack. It was related to snow thinning of 0.1 to 0.2 m, despite of 0.08 m of snow fall. According to our measurements, the contributions of the increase in snow density (0.09 ± 0.06 m), melt (0.08 ± 0.05 m), and evaporation (0.05 ± 0.02 m) were approximately equally important for the observed snow thinning. Accordingly, although December 2004 in the western Weddell Sea was probably warmer than the climatological mean from 1979 to 2005 [*Bareiss and Görgen*, 2008], the atmospheric forcing was not enough to melt the snowpack on sea ice during December, but the final snowmelt must have taken place later in the summer and at lower latitudes where the sea ice was advected. The melt of sea ice itself is mostly due to the heat flux from the ocean [*McPhee*, 2008; *Haas et al.*, 2008].

[60] Important factors for the reduced melt were the high surface albedo and weak winds. The decrease in albedo in December was not enough to trigger any significant positive feedback effect on the snowmelt. This was also due to periods of snow fall and drift, which temporarily increased the albedo. Although the air masses observed at ISPOL mostly originated from warmer climate zones, the winds were weak and the air masses cooled during their long fetch over sea ice. Hence warm air advection was not an important factor for the heat supply to the snowpack on the ISPOL floe, although it probably was important 100 km further north, closer to the ice edge (Nicolaus et al., submitted manuscript, 2009). Also, closer to the Antarctic Peninsula warm, dry Föhn winds are important in both evaporating and melting the snow, as *King et al.* [2008] observed over the Larsen Ice Shelf. Over sea ice this has been observed at least in the Baltic Sea [*Granskog et al.*, 2006].

[61] At nighttime, the turbulent fluxes were very small in magnitude, and the surface temperature was therefore controlled by the incoming longwave radiation. Further, under a certain shortwave radiation, the minimum surface temperature was obtained when the incoming longwave radiation was small, and the turbulent fluxes transported heat from the surface to the atmosphere. This was typically the case under reduced cloud cover, and the minimum surface temperature was controlled by the incoming shortwave radiation.

[62] For most of the year the sensible heat flux over Antarctic sea ice is from air to snow, but in summer both upward and downward fluxes have been observed, and the ISPOL results on predominantly upward fluxes may not be generalized for the entire Antarctic sea ice zone. More extensive observations are needed to answer the remaining questions: (1) what is the typical direction of the sensible heat flux in summer, (2) over how long period upward fluxes can be observed, and (3) how large are the regional differences within the Antarctic sea ice zone?

[63] Little attention has previously been paid on the diurnal cycle of atmospheric variables and surface fluxes in the Antarctic sea ice zone. The ISPOL data demonstrated that a clear diurnal cycle was present in 15 quantities and, for example, in the surface albedo in melting conditions the diurnal cycle was almost as large as the seasonal change through the study period. Our result for the instantaneous net heat flux to the snowpack had an error margin of approximately ± 10 W m^{-2}. Comparing this to the time series in Figure 8, we can be confident that the snowpack was receiving heat every day, while it was releasing heat for at least a short period every night. This generated a diurnal cycle of melt and refreezing, and further caused snow metamorphosis with increasing grain size and formation of ice layers (Nicolaus et al., submitted manuscript, 2009). Further quantification of these processes is essential, among others, for the interpretation of the onset of snowmelt on the basis of remote sensing data [*Willmes et al.*, 2006, 2007]. Quantitative reproduction of the diurnal cycle is also a challenge for atmospheric models [*Steeneveld et al.*, 2008].

[64] Comparisons between ISPOL, SHEBA, and AOE-2001 results demonstrated large differences in the summertime surface heat budget over the Antarctic and Arctic sea ice. In ISPOL, the air was colder, surface albedo remained higher, and a larger portion of the absorbed solar radiation was returned to the atmosphere via the turbulent heat fluxes. The limited melt allowed a larger diurnal cycle in the surface temperature, which affected several atmospheric variables including the base height of low clouds. The differences in summer conditions within the Antarctic sea ice zone can, however, at least temporarily be even larger than between ISPOL and SHEBA (Figure 11), and distinguishing between spatial and temporal variations on the basis of limited observations remains a challenge.

[65] In any case, supported by remote sensing data [*Willmes et al.*, 2006, 2007], the ISPOL observations on a thick snow cover, high albedo, small net heat flux, and late onset of melting suggest that effective surface melt of Antarctic sea ice can only take place at the northernmost parts of the sea ice zone.

[66] **Acknowledgments.** We thank the captain and crew of *R/V Polarstern* and the other scientists at ISPOL for their continuous support. In particular, Jörg Bareiss, Pekka Kosloff, Marcel Nicolaus, and Sascha Willmes are acknowledged for their collaboration in the field work and data quality control. We thank Christian Haas and another reviewer for their constructive comments on the manuscript, and Roberta Pirazzini for fruitful discussions. The research was funded by the Academy of Finland grants 78458 and 210794, and the Finnish Antarctic Research Programme (FINNARP) supported the field work.

References

Andreas, E. L. (1985), Heat and moisture advection over Antarctic Sea ice, *Mon. Weather Rev.*, *113*, 736–746.

Andreas, E. L. (1987), A theory for the scalar roughness and the scalar transfer coefficients over snow and sea ice, *Boundary Layer Meteorol.*, *38*, 159–184.

Andreas, E. L., and A. P. Makshtas (1985), Energy exchange over Antarctic sea ice in the spring, *J. Geophys. Res.*, *90*, 7199–7212.

Andreas, E. L., K. J. Claffey, and A. P. Makshtas (2000), Low-level atmospheric jets and inversions over the western Weddell Sea, *Boundary Layer Meteorol.*, *97*, 459–486.

Andreas, E. L., R. E. Jordan, and A. P. Makshtas (2004), Simulations of snow, ice, and near-surface atmospheric processes on ice Station Weddell, *J. Hydrometeorol.*, *5*, 611–624.

Andreas, E. L., R. E. Jordan, and A. P. Makshtas (2005), Parameterizing turbulent exchange over sea ice: The Ice Station Weddell results, *Boundary Layer Meteorol.*, *114*, 439–460.

Bareiss, J., and K. Görgen (2008), ISPOL weather conditions in the context of long-term climate variability in the north-western Weddell Sea, *Deep Sea Res. II*, *55*, 918–932.

Brandt, R. E., S. G. Warren, A. P. Worby, and T. C. Grenfell (2005), Surface albedo of the Antarctic Sea ice zone, *J. Clim.*, *18*, 3606–3622.

Brümmer, B., D. Schröder, J. Launiainen, T. Vihma, A.-S. Smedman, and M. Magnusson (2002), Temporal and spatial variability of surface fluxes over the ice edge zone in the northern Baltic Sea, *J. Geophys. Res.*, *107*(C8), 3096, doi:10.1029/2001JC000884.

Fairall, C. W., P. O. G. Persson, E. F. Bradley, R. E. Payne, and S. P. Anderson (1998), A new look at calibration and use of Eppley precision infrared radiometers. part I: Theory and application, *J. Atmos. Ocean. Technol.*, *15*, 1229–1242.

Grachev, A. A., C. W. Fairall, P. O. G. Persson, E. L. Andreas, and P. S. Guest (2005), Stable boundary-layer scaling regimes: The Sheba data, *Boundary Layer Meteorol.*, *116*, 201–235.

Granskog, M., T. Vihma, R. Pirazzini, and B. Cheng (2006), Superimposed ice formation and surface fluxes on sea ice during the spring melt-freeze period in the Baltic Sea, *J. Glaciol.*, *52*, 119–127.

Grenfell, T. C., and D. K. Perovich (2004), Seasonal and spatial evolution of albedo in a snow-ice-land-ocean environment, *J. Geophys. Res.*, *109*(C1), C01001, doi:10.1029/2003JC001866.

Guest, P. S. (2007), Measuring turbulent heat fluxes over leads using kites, *J. Geophys. Res.*, *112*, C05021, doi:10.1029/2006JC003689.

Haas, C. (2003), Dynamics versus thermodynamics, in *Sea Ice: An Introduction to Its Physics, Chemistry, Biology and Geology*, edited by D. N. Thomas and G. S. Dieckmann, pp. 82–111, Blackwell, Malden, Mass.

Haas, C., M. Nicolaus, S. Willmes, A. P. Worby, and D. Flinspach (2008), Sea ice and snow thickness and physical properties of an ice floe in the western Weddell Sea and their changes during spring warming, *Deep Sea Res. II*, *55*, 963–974.

Heil, P., J. K. Hutchings, A. P. Worby, M. Johansson, J. Launiainen, C. Haas, and W. D. Hibler III (2008), Tidal forcing on sea-ice drift and deformation in the western Weddell Sea in early austral summer, 2004, *Deep Sea Res. II*, *55*, 943–962.

Hellmer, H. H., C. Haas, G. S. Dieckmann, and M. Schröder (2006), Sea ice feedbacks observed in the western Weddell Sea, *Eos Trans. AGU*, *87*, 173–184.

Hellmer, H. H., M. Schröder, C. Haas, G. S. Dieckmann, and M. Spindler (2008), The ISPOL drift experiment, *Deep Sea Res. II*, *55*, 913–917.

Högström, U. (1988), Non-dimensional wind and temperature profiles in the atmospheric surface layer: A re-evaluation, *Boundary Layer Meteorol.*, *42*, 55–78.

Holtslag, A. A. M., and H. A. R. de Bruin (1988), Applied modelling of the nighttime surface energy balance over land, *J. Appl. Meteorol.*, *37*, 689–704.

King, J. C., T. A. Lachlan-Cope, R. S. Ladkin, and A. Weiss (2008), Airborne measurements in the stable boundary layer over the Larsen Ice Shelf, Antarctica, *Boundary Layer Meteorol.*, *127*(3), 413–428.

Kohsiek, W., C. Liebethal, T. Foken, R. Vogt, S. P. Oncley, C. Bernhofer, and H. A. R. De Bruin (2007), The Energy Balance Experiment EBEX-2000: part III. Behaviour and quality of the radiation measurements, *Boundary Layer Meteorol.*, *123*, 55–75, doi:10.1007/s10546-006-9135-8.

Kottmeier, C., and D. Engelbart (1992), Generation and atmospheric heat exchange of coastal polynyas in the Weddell Sea, *Boundary Layer Meteorol.*, *60*, 207–234.

Launiainen, J. (1995), Derivation of the relationship between the Obukhov stability parameter and the bulk Richardson number for flux-profile studies, *Bound. Layer Meteorol.*, *76*, 165–179.

Launiainen, J., and T. Vihma (1990), Derivation of turbulent surface fluxes - an iterative flux-profile method allowing arbitrary observing heights, *Environ. Software*, *5*, 1–15.

Launiainen, J., and T. Vihma (1994), On the surface heat fluxes in the Weddell Sea, in *The Polar Oceans and Their Role in Shaping the Global Environment, Nansen Centennial Volume*, *Geophys. Monogr. Ser.*, vol. 85, edited by O. M. Johannessen, R. Muench, and J. E. Overland, pp. 399–419, AGU, Washington, D. C.

Launiainen, J., T. Vihma, J. Aho, and K. Rantanen (1991), Air-Sea Interaction Experiment in the Weddell Sea. Argos-Buoy Report from FINNARP-5/89, 1990–1991, Antarctic Reports of Finland, *Rep. 2*, 27 + 19 pp., Ministry of Trade and Industry, Helsinki.

Launiainen, J., M. Johansson, and P. Kosloff (2007), Meteorological conditions and surface fluxes and energy balance during ISPOL, in *The Expeditions ANTARKTIS-XXII/1 and XXII/2 of the Research Vessel Polarstern in 2004/2005*, edited by S. El Naggar et al., *Rep. Polar Mar. Res. 551*, pp. 53–66, Alfred Wegener Institute for Polar and Marine Research, Bremerhaven, Germany.

Mahrt, L. (2002), Stably stratified boundary layer, in *Encyclopedia of Atmospheric Sciences*, edited by J. P. Holton, J. A. Curry, and J. Pyle, pp. 298–305, Elsevier, New York.

Martinson, D. G., and R. A. Iannuzzi (1998), Antarctic ocean-ice interaction: Implications from ocean bulk property distributions in the Weddell Gyre, in *Antarctic Sea Ice: Physical Processes, Interactions and Variability*, *Antarctic Res. Ser.*, vol. 74, edited by M. O. Jeffries, AGU, Washington, D. C.

McPhee, M. G. (2008), Physics of early summer ice/ocean exchanges in the western Weddell Sea during ISPOL, *Deep Sea Res. II*, *55*, 1075–1097.

Nicolaus, M., C. Haas, J. Bareiss, and S. Willmes (2006), A model study of differences of snow thinning on Arctic and Antarctic first-year sea ice during spring and summer, *Ann. Glaciol.*, *44*, 147–153.

Niros, A., T. Vihma, and J. Launiainen (2002), Marine meteorological conditions and air-sea exchange processes over the Baltic Sea in 1990s, *Geophysica*, *38*, 59–87.

Parkinson, C. L. (2004), Southern Ocean sea ice and its wider linkages: Insights revealed from models and observations, *Antarctic Sci.*, *16*, 387–400.

Perovich, D. K. (1996), The optical properties of sea ice, *Monogr., 96-1*, U. S. Army Corps of Eng., Cold Reg. Res. and Eng. Lab., Hanover, N. H., 24 pp.

Persson, P. O. G., C. W. Fairall, E. L. Andreas, P. S. Guest, and D. K. Perovich (2002), Measurements near the atmospheric surface flux group tower at SHEBA: Near-surface conditions and surface energy budget, *J. Geophys. Res.*, *107*(C10), 8045, doi:10.1029/2000JC000705.

Pirazzini, R. (2004), Surface albedo measurements over Antarctic sites in summer, *J. Geophys. Res.*, *109*, D20118, doi:10.1029/2004JD004617.

Pirazzini, R., T. Vihma, M. A. Granskog, and B. Cheng (2006), Surface albedo measurements over sea ice in the Baltic Sea during the spring snowmelt period, *Ann. Glaciol.*, *44*, 7–14.

Schmidt, T., and G. König-Langlo (1994), Radiation measurements at the German Antarctic Station Neumayer 1982–1992, *Rep. Polar. Res.*, vol. 146, 65 pp., Alfred Wegener Institute for Polar and Marine Res., Bremerhaven, Germany.

Steeneveld, G. J., T. Mauritsen, E. I. F. de Bruijn, J. Vila-Guerau de Arellano, G. Svensson, and A. A. M. Holtslag (2008), Evaluation of limited-area models for the representation of the diurnal cycle and contrasting nights in CASES-99, *J. Appl. Meteorol. Climatol.*, *47*, 869–887.

Steer, A., A. Worby, and P. Heil (2008), Observed changes in sea-ice floe size distribution during early summer in the western Weddell Sea, *Deep Sea Res. II*, *55*, 933–942.

Stössel, A., W.-G. Cheon, and T. Vihma (2008), Interactive momentum flux forcing over sea ice in a global ocean GCM, *J. Geophys. Res.*, *113*, C05010, doi:10.1029/2007JC004173.

Thomas, D. N., and G. S. Dieckmann (Eds.) (2003), *Sea Ice: An Introduction to Its Physics, Chemistry, Biology and Geology*, 402 pp., Blackwell, Malden, Mass.

Tietäväinen, H., and T. Vihma (2008), Atmospheric moisture budget over Antarctica and Southern Ocean on the basis of ERA-40 reanalysis, *Int. J. Climatol.*, *28*, 1977–1995, doi:10.1002/joc.1684.

Tisler, P., T. Vihma, G. Müller, and B. Brümmer (2008), Modelling of warm-air advection over Arctic sea ice, *Tellus*, *60A*, 775–788.

Tison, J.-L., A. Worby, B. Delille, F. Brabant, S. Papadimitriou, D. Thomas, J. de Jong, D. Lannuzel, and C. Haas (2008), Temporal evolution of decaying summer first year sea ice in the western Weddell Sea, Antarctica, *Deep-Sea Res. II*, *55*, 1075–1097.

Tjernström, M. (2005), The summer Arctic boundary layer during the Arctic Ocean Experiment 2001 (AOE-2001), *Boundary Layer Meteorol.*, *117*, 5–36.

Tjernström, M. (2007), Is there a diurnal cycle in the summer cloud-capped Arctic boundary layer?, *J. Atmos. Sci.*, *64*, 3970–3986.

Valkonen, T., T. Vihma, and M. Doble (2008), Mesoscale modeling of the atmosphere over Antarctic sea ice: A late-autumn case study, *Mon. Weather Rev.*, *136*, 1457–1474.

Van den Broeke, M., C. Reijmer, and R. Van de Wal (2004), Surface radiation balance in Antarctica as measured with automatic weather stations, *J. Geophys. Res.*, *109*, D09103, doi:10.1029/2003JD004394.

Van de Wiel, B. J. H., A. F. Moene, G. J. Steeneveld, O. K. Hartogensis, and A. A. M. Holtslag (2007), Predicting the collapse of turbulence in stably stratified boundary layers, *Flow Turbul. Combust.*, *79*, 251–274, doi: 10.1007/s10494-007-9094-2.

Vihma, T., J. Launiainen, and J. Uotila (1996), Weddell Sea ice drift: Kinematics and wind forcing, *J. Geophys. Res.*, *101*, 18,279–18,296.

Vihma, T., J. Uotila, B. Cheng, and J. Launiainen (2002), Surface heat budget over the Weddell Sea: Buoy results and comparisons with large-scale models, *J. Geophys. Res.*, *107*(C2), 3013, doi:10.1029/2000JC000037.

Vihma, T., C. Lüpkes, J. Hartmann, and H. Savijärvi (2005), Observations and modelling of cold-air advection over Arctic sea ice in winter, *Boundary Layer Meteorol.*, *117*, 275–300.

Willmes, S., J. Bareiss, C. Haas, and M. Nicolaus (2006), The importance of diurnal processes for the seasonal cycle of sea-ice microwave brightness temperatures during early summer in the Weddell Sea, Antarctica, *Ann. Glaciol.*, *44*, 297–302.

Willmes, S., J. Bareiss, and C. Haas (2007), New data set of onset of annual snowmelt on Antarctic sea ice, *Eos Trans. AGU*, *88*, 237–241.

Wendler, G., and A. P. Worby (2001), The surface energy budget in the Antarctic summer sea-ice pack, *Ann. Glaciol.*, *33*, 275–279.

Wendler, G., U. Adolphs, A. Hauser, and B. Moore (1997), On the surface energy budget of sea ice, *J. Glaciol.*, *43*, 122–130.

Wendler, G., B. Hartmann, C. Wyatt, M. Shulski, and H. Stone (2005), Midsummer energy balance for the southern seas, *Boundary Layer Meteorol.*, *117*, 131–148.

Zeng, J., Y. Tohjima, Y. Fujinuma, H. Mukai, and M. Katsumoto (2003), A study of trajectory quality using methane measurements from Hateruma Island, *Atmos. Environ.*, *37*, 1911–1919.

M. M. Johansson and J. Launiainen, Marine Research, Finnish Meteorological Institute, P. O. Box 503, Erik Palmenin aukio 1, FI-00101 Helsinki, Finland.

T. Vihma, Meteorological Research, Finnish Meteorological Institute, P.O. Box 503, Erik Palmenin aukio 1, F-00101 Helsinki, Finland. (timo.vihma@fmi.fi)